

**The Nature of Compact Galaxies in the Hubble Deep Field — II:  
Spectroscopic Properties and Implications for the Evolution of  
the Star Formation Rate Density of the Universe.** <sup>1,2,3</sup>

Rafael Guzmán, Jesús Gallego, David C. Koo, Andrew C. Phillips, James D. Lowenthal<sup>4</sup>,  
S. M. Faber, Garth D. Illingworth & Nicole P. Vogt  
University of California Observatories / Lick Observatory,  
Board of Studies in Astronomy and Astrophysics,  
University of California, Santa Cruz, CA 95064

Received .....; accepted .....

To be submitted to *Astrophysical Journal*

---

<sup>1</sup>Based on observations obtained at the W. M. Keck Observatory, which is operated jointly by the University of California and the California Institute of Technology.

<sup>2</sup>Based in part on observations with the NASA/ESA *Hubble Space Telescope*, obtained at the Space Telescope Science Institute, which is operated by AURA under NASA contract NAS 5-26555.

<sup>3</sup>Lick Observatory Bulletin No.000

<sup>4</sup>Hubble Fellow

We present a spectroscopic study of 51 compact field galaxies with redshifts  $z < 1.4$  and apparent magnitudes  $I_{814} < 23.74$  in the flanking fields of the Hubble Deep Field. These galaxies are compact in the sense that they have small apparent half-light radii ( $r_{1/2} \leq 0.5$  arcsec) and high surface brightnesses ( $\mu_{I814} \leq 22.2$  mag arcsec $^{-2}$ ). The spectra, taken at the Keck telescope, show emission lines in 88% of our sample, and only absorption lines in the remaining 12%. Emission-line profiles are roughly Gaussian with velocity widths that range from the measurement limit of  $\sigma \sim 35$  km s $^{-1}$  to 150 km s $^{-1}$ . Rest-frame [OII] $\lambda$ 3727 equivalent widths range from 5Å to 94Å, yielding star formation rates (SFR) of  $\sim 0.1$  to 14  $M_{\odot}$  yr $^{-1}$ . The analysis of various line diagnostic diagrams reveals that  $\sim 60\%$  of compact emission-line galaxies have velocity widths, excitations, H $\beta$  luminosities, SFRs, and mass-to-light ratios characteristic of young star-forming HII galaxies. The remaining 40% form a more heterogeneous class of evolved starbursts, similar to local starburst disk galaxies. We find that, although the compact galaxies at  $z > 0.7$  have similar SFRs per unit mass to those at  $z < 0.7$ , they are on average  $\sim 10$  times *more massive*. Our sample implies a lower limit for the global comoving SFR density of  $\sim 0.004$   $M_{\odot}$  yr $^{-1}$  Mpc $^{-3}$  at  $z = 0.55$ , and  $\sim 0.008$   $M_{\odot}$  yr $^{-1}$  Mpc $^{-3}$  at  $z = 0.85$  (assuming Salpeter IMF,  $H_0 = 50$  km s $^{-1}$  Mpc $^{-1}$ , and  $q_0 = 0.5$ ). These values, when compared to estimates for a sample of local compact galaxies selected in a similar fashion, support a history of the universe in which the SFR density declines by a factor  $\sim 10$  from  $z = 1$  to today. From the comparison with the SFR densities derived for magnitude-limited samples of field galaxies, we conclude that compact emission-line galaxies, though only  $\sim 20\%$  of the general field population, may contribute as much as  $\sim 45\%$  to the global SFR of the universe at  $0.4 < z < 1$ .

*Subject headings:* galaxies: formation — galaxies: compact — galaxies: evolution — galaxies: fundamental parameters — cosmology: observations

## 1. Introduction

Faint compact galaxies are relevant to observational cosmology because they serve to constrain several proposed explanations of the abundance of faint blue field galaxies (see reviews by Koo and Kron 1992; Lilly 1993; Ellis 1996). These include models with large populations of low-luminosity dwarfs at low redshifts (Phillipps & Driver 1995); bursting dwarfs at  $z < 1$  that have faded or disappeared by today (Cowie, Songaila & Hu 1991; Babul & Ferguson 1996); low-luminosity AGN's (Tresse *et al.* 1996); or smaller pre-merger components (Guiderdoni & Rocca-Volmerange 1990; Broadhurst *et al.* 1992; Kauffmann *et al.* 1993; Cole *et al.* 1994). Faint compact galaxies are also likely to include compact narrow emission-line galaxies (CNELGs), which are starbursts at moderate redshifts that have been proposed to be progenitors of today's spheroidal galaxies like NGC 205 (Koo *et al.* 1994, 1995; Guzmán *et al.* 1996). Given their likely starburst nature, faint compact galaxies may be major contributors to the global star formation rate (SFR) density already found to increase with lookback time to at least redshift  $z \sim 1$  (Cowie *et al.* 1995, Lilly *et al.* 1996).

Most compact galaxies at moderate redshifts yield little morphological information, even in HST images. Their integrated spectra are thus particularly valuable in providing information on their galaxy type, kinematics, and stellar content, as well as the physical conditions of the ionized gas and star formation activity. In this pair of papers, we study the properties of a sample of 51 faint compact galaxies in the flanking fields of the Hubble Deep Field (HDF; Williams *et al.* 1996). The global properties of our sample are described by Phillips *et al.* (1997; hereafter Paper I), who find that the majority of faint compact galaxies tends to have colors, luminosities, half-light radii, surface brightnesses, and mass-to-light ratios consistent with those of local vigorously star-forming galaxies. In this paper, we focus our analysis on their spectroscopic properties. The wide spectral range (4000-9000Å)

and good resolution ( $\sim 4\text{\AA}$  FWHM) of our survey offer significant advantages for a spectral analysis of compact field galaxies at intermediate redshifts. Most spectroscopic surveys of faint galaxies do not cover the entire optical wavelength range, hence emission-line studies have been restricted mainly to the [OII] $\lambda 3727$  doublet (e.g., Broadhurst *et al.* 1988; Colless *et al.* 1990; Glazebrook *et al.* 1995). At  $z < 0.7$ , we can reliably measure not only [OII] $\lambda 3727$  but also [OIII] $\lambda 4959$ , [OIII] $\lambda 5007$ , and  $H\beta$ . Flux ratios among these lines provide powerful diagnostics to discriminate among different classes of emission-line galaxies (Baldwin, Phillips & Terlevich 1981; Veilleux & Osterbrock 1987). For example, a recent study of line ratios for field galaxies at  $z < 0.3$  suggests that at least 8% are active galaxies such as Seyfert 2 or LINERS (Tresse *et al.* 1996). A second major distinguishing feature of the present study is the inclusion of velocity width measurements from emission lines. Internal velocities, as inferred from the motions of the ionized gas, have proven to be very useful in understanding the nature of distant field galaxies and assessing their evolutionary state (Koo *et al.* 1995; Forbes *et al.* 1996; Guzmán *et al.* 1996; Vogt *et al.* 1996; Rix *et al.* 1997). Together with other spectroscopic parameters such as the excitation of the ionized gas,  $H\beta$  luminosity, and current SFR, the new velocity widths improve discrimination among different classes of emission-line galaxies and provide a more reliable comparison to potential local counterparts.

This paper is organized as follows. In Section 2 we describe briefly our sample selection and spectroscopic observations. In Section 3 we describe the emission-line measurements. In Section 4 we study the nature of the compact emission-line galaxies. In Section 5 we derive the comoving SFR density at  $0.4 \leq z \leq 1.0$  for our sample and compare our results to previous observations and model predictions. The main results of this paper are summarized in Section 6. Throughout this paper we adopt  $H_0 = 50 \text{ km s}^{-1} \text{ Mpc}^{-1}$  and  $q_0 = 0.05$ , unless otherwise stated. Given these parameters,  $L^*$  ( $M_B \sim -21$ ) corresponds to  $I_{814} \sim 21$  and  $1''$  spans 9 kpc at a redshift of  $z = 0.7$ . This project is part of the DEEP

program (Koo 1995).

## 2. Description of the sample and observations

The galaxy sample was selected from  $I_{814}$  HST images of the flanking fields around the HDF (Williams *et al.* 1996). A full description of the sample selection, spectroscopic observations, and measurements of photometric parameters is given in Paper I. Briefly, these galaxies were chosen to have  $I_{814} \leq 23.74$ , half-light radius  $r_{1/2} \leq 0.5$  arcsec, and average surface brightness within the half-light radius  $\mu_{I_{814}} \leq 22.2$  mag arcsec<sup>-2</sup>. Hereafter we refer to this sample as *compact galaxies*. Stellar-like objects with  $r_{1/2} \leq 0.16$  arcsec were rejected. Spectra were obtained using the Low-Resolution Imaging Spectrograph (Oke *et al.* 1995) at the W. M. Keck Telescope in UT April 22-24, 1996. The seeing was typically  $\sim 0.8$  arcsec. With a slitwidth of 1.1 arcsec, a 600 l/mm grating yielded an instrumental resolution of  $\sim 4$  Å FWHM at  $1.26$  Å pix<sup>-1</sup>. However, since our objects have  $r_{1/2} \leq 0.5$  arcsec, the effective resolution is estimated to be  $\sim 3.1$  Å (see Paper I). Total exposure times were 3000s at each of two gratings setups (blue and red). The total spectral range is  $\sim 4000$ - $9000$  Å, with the exact range depending on the position of the target on the mask. The spectroscopic reduction included the usual corrections for bias, dark current, flatfield, and cosmic rays as well as wavelength calibration and background sky subtraction. No flux calibration was attempted. The final one-dimensional spectra were produced by coadding the central 6 pixels (1.3 arcsec) for each object. The analysis presented in this paper refers to the sub-sample of 51 compact galaxies with measured  $V - I$  colors and redshift identifications with  $z < 2$ . We have also excluded one nearly stellar-like object (iw3\_0817\_0556 at  $z=0.960$ ) with broad MgII $\lambda$ 2795,2803 emission lines (rest-frame FWHM  $\sim 23$ Å) similar to those found in low-luminosity QSOs or Seyfert galaxies (see Appendix to Paper I).

Figure 1 shows five representative spectra. Of the 51 compact galaxies, 6 (or 12%) show absorption-line spectra characteristic of elliptical and S0 galaxies (Figure 1a). The major features displayed in these spectra are blended stellar absorption lines in the continuum dominated by K-giant stars, including the 4000 Å Ca H + K break, G-band, Mgb and Na D features. Except for iw4\_1173\_1391, which shows marginal emission in [OII] $\lambda$ 3727, there is no evidence for any nebular emission within the observed wavelength range. The remaining 45 galaxies (88%) exhibit prominent nebular oxygen and/or Balmer emission lines, and blue continua characteristic of vigorous star-forming systems or narrow-line active galactic nuclei. A large fraction have spectra that resemble those of star-forming HII regions (Figures 1b and 1c), showing narrow lines and a wide range in excitation as evidenced by the [OIII] $\lambda$ 5007/H $\beta$  flux ratio. Particularly interesting are the spectra of seven galaxies at  $z > 0.7$  showing strong [OII] $\lambda$ 3727 lines, and a strong continuum bluewards of [OII] $\lambda$ 3727 with clear FeII  $\lambda$ 2600 and MgII  $\lambda$ 2796 absorption features (Figure 1d). These features are characteristic of extreme local starburst galaxies such as NGC 2415 or NGC 5253, which are undergoing a very recent violent episode of star formation (Kinney *et al.* 1996). Two other galaxies, also at  $z > 0.7$ , have similar blue continuum but show unusually narrow MgII $\lambda$ 2796 emission (restframe FWHM  $\sim 3.5$  Å) with P-Cygni line profiles, as well as strong [OII] $\lambda$ 3727 and [NeIII] $\lambda$ 3869, and weak narrow H $\gamma$  and H $\delta$  emission lines (Figure 1e). Although the narrow lines argue against nuclear activity in these objects, we have not been able to find similar spectral characteristics in the UV spectra of local starbursts. A more quantitative analysis of the general spectroscopic properties of the emission-line compact galaxies is presented in Section 4.

### 3. Emission-line Measurements

Paper I shows that the redshift distribution of compact galaxies parallels that of typical field galaxies in the HDF and is roughly bimodal with peaks around  $z \sim 0.5$  and  $z \sim 0.9$ . We thus divide our objects into ‘intermediate- $z$ ’ (26 emission-line galaxies at  $z < 0.7$ ) and ‘high- $z$ ’ (19 emission-line galaxies at  $z > 0.7$ ) samples. The main spectral features seen in the intermediate sample are: [OII] $\lambda$ 3726,3729, H $\beta$ , [OIII] $\lambda$ 4959, and [OIII] $\lambda$ 5007. Four objects at  $z < 0.4$  also exhibit other emission lines such as HeI $\lambda$ 5876, H $\alpha$ , [NII] $\lambda$ 6548,6583, and [SII] $\lambda$ 6717,6731. For the high- $z$  sample ( $z > 0.7$ ), the [OII] doublet is generally the only major feature that can be reliably measured. The emission-line measurements described below refer to the strongest features most commonly observed in our spectra, i.e., [OII] $\lambda$ 3726,3729, H $\beta$ , and [OIII] $\lambda$ 5007 (hereafter referred to as [OII], H $\beta$  and [OIII], respectively).

#### 3.1. Equivalent Widths

Equivalent widths (EW) were measured by fitting a Gaussian function to the emission-line profiles using the SPLOT program in IRAF<sup>5</sup>. The continuum levels and the range over which the fits were performed were set interactively, with repeat measurements made in difficult cases. The effective instrumental resolution of 3.1Å resolves the [OII] doublet in  $\sim 25\%$  of the spectra. In all cases, the standard deblending routine within SPLOT was used to fit both components. The FWHM for the two-Gaussian fit were forced to be equal, and the distance in wavelength between the two centroids was fixed to the theoretical value

---

<sup>5</sup>IRAF is distributed by the National Optical Astronomy Observatories, which is operated by the Association of Universities for Research in Astronomy, Inc. (AURA) under cooperative agreement with the National Science Foundation

( $2.75 \times (1 + z) \text{ \AA}$ ). All lines, whether double or single, were generally well-fitted by Gaussian profiles. EW's were measured from direct integration of the flux given by the Gaussian fit in the rest frame. No correction for stellar absorption was made to the measured EW of H $\beta$ . This correction amounts typically to  $\sim 2\text{-}5 \text{ \AA}$  for HII galaxies and spiral galaxies (Tresse *et al.* 1996; Kennicutt 1992). For the [OII] doublet, we coadded the flux of each line to give a single measure of EW that can be directly compared to that commonly measured at lower spectral resolution. All EW measurements were derived independently using software designed by one of us (ACP), which directly integrated the flux in the line. Comparing both techniques, we estimate that the average uncertainty of our measurements is  $\sim 15\%$ . The histograms of  $EW_{[OII]}$  in the rest-frame for the intermediate and high- $z$  samples are shown in Figure 2a. These values range from 5  $\text{ \AA}$  to 94  $\text{ \AA}$  with an average of 43  $\text{ \AA}$  (rms = 24 $\text{ \AA}$ ). Note that there is no significant difference in the distribution of  $EW_{[OII]}$  between both redshift samples. Using the two-sided Kolmogorov-Smirnov test, the probability is  $\sim 82\%$  for the intermediate- and high- $z$  samples to be drawn from the same parent distribution.

### 3.2. Velocity Widths

Velocity widths ( $\sigma$ ) were characterized as the rms velocity dispersion of the Gaussian fit to a given line with rest-frame wavelength  $\lambda_i$ , corrected for redshift and instrumental resolution, i.e.:

$$\sigma_i = \sqrt{\text{FWHM}_i^2 - (3.1 \text{ \AA})^2} \times \frac{3 \times 10^5 \text{ km s}^{-1}}{2.35 \lambda_i (1 + z)}$$

Most of the emission-lines in our spectra do not deviate significantly from the Gaussian fit. These profiles are consistent with those measured in high resolution, high signal-to-noise spectra of a similar sample of compact, narrow emission-line galaxies (Koo *et al.* 1995; Guzmán *et al.* 1996). We estimate that the lowest  $\sigma_i$  value that can be reliably measured



with our instrumental resolution is  $\sim 35 \text{ km s}^{-1}$  (at a 90% confidence level). Individual  $\sigma_i$  measurements were assigned a quality parameter  $Q$  related to the signal-to-noise ratio (SNR) per  $\text{\AA}$  of each line. We adopted  $Q=1$  for  $\text{SNR} \leq 20$ ,  $Q=2$  for  $20 < \text{SNR} < 40$ , and  $Q=3$  for  $\text{SNR} \geq 40$ . A total of 48 objects have at least one  $\sigma_i$  measurement with  $Q > 1$ . No significant systematic difference among  $\sigma_i$  measurements from various lines of the same object was found, although we note that the velocity widths derived from [OII] are  $\sim 15\% \pm 8\%$  higher than those values derived from [OIII] and  $\text{H}\beta$ . From the variance among different line measurements for the same galaxy, the typical uncertainty of an individual  $\sigma_i$  measurement is  $\sim 20\%$ . The quality code was used to derive a final  $\sigma$  value as the weighted average of the values for all available emission lines given by the expression:

$$\sigma = \frac{\sum_i Q_i \sigma_i}{\sum_i Q_i}$$

The uncertainty in the final measurements is typically  $\sim 15\%$ .

Figure 2b shows the histograms of  $\sigma$  measurements for the intermediate and high- $z$  samples. The  $\sigma$  values range from about  $35 \text{ km s}^{-1}$  (the measurement limit) to  $150 \text{ km s}^{-1}$ , with an average value of  $65 \text{ km s}^{-1}$  ( $\text{rms} = 29 \text{ km s}^{-1}$ ). In contrast to the  $EW_{[\text{OII}]}$  histogram, the  $\sigma$  distribution shows significant differences with redshift in the sense that galaxies at  $z > 0.7$  have, on average,  $40\% \pm 10\%$  larger  $\sigma$  than those at  $z \leq 0.7$ . This effect is not due to the small systematic offset of  $\sim 8\%$  between [OII]-based velocity widths (used exclusively for the high- $z$  sample) and the average velocity widths adopted for the intermediate sample. Using the two-sided K-S test, the probability that both distributions are drawn from the same parent distribution is only  $\sim 1\%$ .

### 3.3. Excitation and $H\beta$ luminosities

A useful indicator of the physical conditions of the ionized gas is the  $[\text{OIII}]\lambda 5007$  to  $H\beta$  flux ratio (so-called *excitation*). The proximity in wavelength between  $H\beta$  and  $[\text{OIII}]$  ensures that any extinction correction in this ratio is small. Unfortunately, for some galaxies at  $z < 0.7$ , one or both lines lie close to strong sky emission lines which prevented reliable measurements. In total,  $[\text{OIII}]\lambda 5007/H\beta$  could be measured for only 24 galaxies, mostly at  $z \leq 0.7$ . For 28 galaxies we have also derived  $H\beta$  luminosities from the measured rest-frame equivalent widths  $EW_{H\beta}$  and absolute B magnitudes (see Terlevich & Melnick 1981). In principle, these luminosities need to be corrected for internal extinction and stellar absorption. For local star-forming galaxies, these two corrections typically amount to  $\sim 0.8$  dex and  $\sim 0.1$  dex, respectively. Since their size is very uncertain for our sample, we will not apply any such corrections to the observed  $H\beta$  luminosities of compact galaxies. Comparison with local samples will be made using only un-corrected values for the nearby galaxies.

### 3.4. Star Formation Rates

We have estimated the SFR based on  $EW_{[\text{OII}]}$ . Metallic nebular lines like  $[\text{OII}]$  are affected by the physical conditions of the ionized gas (e.g., excitation and metallicity), and the transformation from SFR estimated this way to SFR from  $H\alpha$  fluxes (the best SFR tracer) is not straightforward. Previous studies for local emission-line galaxies by Gallagher *et al.* (1989) and Kennicutt (1992) give expressions for such transformations that differ by a factor  $\sim 5$ . Gallagher *et al.* studied a sample of nearby blue irregulars, while Kennicutt used a sample of nearby galaxies covering all disk galaxy types. The disagreement between the two calibrations may reflect the difference in extinction and reddening between irregulars and spirals, and the different IMF and stellar models used by Kennicutt and Gallagher

*et al.* (Kennicutt 1992). Other factors that may contribute to the observed difference are the possible stronger contribution of extended diffuse ionized gas in irregulars, or variations in the sampling of the disk for the two galaxy types.

In order to estimate the SFR using  $EW_{[OII]}$ , we have derived our own transformation between  $H\alpha$  and  $[OII]$  fluxes using a sample of local emission-line galaxies that best resembles the typical characteristics of our sample. The derivation of such transformation is described in detail in the Appendix. The final expression to estimate the SFR as a function of the observed  $EW_{[OII]}$  for compact galaxies is:

$$SFR(M_{\odot} \text{ yr}^{-1}) \approx 2.5 \times 10^{-12} \times 10^{-0.4(M_B - M_{B\odot})} EW_{[OII]}$$

This estimate is  $\sim 3$  times smaller than that derived by Kennicutt, and  $\sim 1.5$  times larger than that obtained by Gallagher *et al.* Absolute blue magnitudes for our sample are listed in Paper I.

Figure 2c shows the histograms of SFR for the intermediate- and high- $z$  samples. While compact galaxies at  $z < 0.7$  have SFRs  $< 3 M_{\odot} \text{ yr}^{-1}$ , those at higher redshifts have SFRs that span a large range from 2 to  $14 M_{\odot} \text{ yr}^{-1}$ . Since the distribution in  $EW_{[OII]}$  is very similar for both samples (Figure 2a), the observed difference in SFRs mainly reflects the fact that we are selecting more luminous galaxies at higher redshifts. The median luminosities in the intermediate and high redshift samples are  $M_B = -19.4$  and  $-21.0$ , respectively (see Paper I). In other words, the average SFR *per unit luminosity* is similar for the intermediate- and high- $z$  samples.

### 3.5. The Data

A complete listing of the emission-line data is given in Table 1. Column (1) lists the galaxy identification. Columns (2) and (3) list the apparent  $I_{814}$  magnitudes and redshifts given in Paper I. The rest-frame equivalent widths of [OII],  $H\beta$ , and [OIII] in  $\text{\AA}$  are listed in columns (4), (5) and (6), respectively. Column (7) lists the excitation. Velocity widths are listed in column (8) in  $\text{km s}^{-1}$ .  $H\beta$  luminosities in  $\text{erg s}^{-1}$ , uncorrected for extinction, are listed in column (9). Star formation rates in  $M_{\odot} \text{ yr}^{-1}$  are listed in column (10). Finally, in column (11) we list the spectral type assigned in Section 4 below.

## 4. Spectroscopic Properties of Compact Emission-Line Galaxies

We investigate the nature of the faint compact galaxies by comparing their spectroscopic properties in various diagnostic diagrams with different types of emission-line galaxies. First, we focus the analysis on two well-known diagrams: excitation vs. luminosity, and  $H\beta$  luminosity vs. velocity width. Together, these diagrams provide insight into the physical characteristics of the ionized gas (e.g., metallicity and internal motions) as well as the strength of any starburst<sup>6</sup>. These plots, however, are useful only for compact galaxies at  $z < 0.7$ , for which  $H\beta$  and [OIII] lie within the observed wavelength range. For galaxies at higher redshift, [OII] is generally the only major feature that can be reliably measured. Since [OII] is a good tracer of the SFR, the  $EW_{[OII]}$  vs. luminosity diagram provides a useful tool to study the star formation characteristics of both the intermediate- and

---

<sup>6</sup>We define “starburst” as a star-forming system with a current SFR that is at least twice the average SFR of normal disk galaxies, which implies a typical  $M/L$  ratio  $\leq 1 M_{\odot}/L_{\odot}$  (cf. Kennicutt, Tamblyn & Congdon 1994). The majority of our galaxies fit this classification (see Paper I).

high- $z$  galaxy samples. We also introduce a new diagram: SFR per unit mass vs. mass. This plot discriminates among various types of star-forming galaxies based solely on their star formation activity, independently of their luminosity. Finally, we propose a broad classification scheme of the compact galaxy sample based on this analysis.

#### 4.1. The Excitation vs. Luminosity Diagram

The spectroscopic properties of narrow emission-line galaxies are generally characterized using line-ratio diagnostic diagrams (Baldwin, Phillips & Terlevich 1981; Veilleux & Osterbrock 1987). Figure 3 shows the  $[\text{OIII}]/\text{H}\beta$  vs.  $M_B$  diagram for the 28 compact galaxies with measured  $[\text{OIII}]/\text{H}\beta$  ratio (squares). All but one (filled square) belong to the intermediate sample ( $z < 0.7$ ). Note that our magnitude limit prevents us from observing galaxies fainter than  $M_B \sim -17$  at  $z > 0.4$  (see Paper I). For comparison, we also plot  $\text{H}\alpha$ -selected emission-line galaxies from the UCM local survey (Gallego *et al.* 1997) and a sample of compact narrow emission-line galaxies (CNELGs) at  $z = 0.1 - 0.7$  studied by Koo *et al.* (1995) and Guzmán *et al.* (1996).

In the  $[\text{OIII}]/\text{H}\beta$  vs.  $M_B$  diagram, local emission-line galaxies can be grouped into two different classes: starburst galaxies and active galaxies (e.g. Salzer *et al.* 1989). The first class consists of objects where the gas is ionized by young O and B stars, and includes starburst nuclei (SBN), dwarf amorphous nuclear starbursts (DANS) and HII galaxies. The second class contains ionization sources harder than hot main sequence stars, such as Seyfert galaxies and LINERS. Local starburst galaxies define a continuous sequence in Figure 3 analogous to the so-called ‘HII’ sequence observed in the  $[\text{OIII}]/\text{H}\beta$  vs.  $[\text{NII}]/\text{H}\alpha$  diagram (Veilleux & Osterbrock 1987). This sequence is interpreted as being a variation in the metallicity content of the ionized gas (Dopita & Evans 1986; Stasinska 1990). Along the HII sequence, metallicity increases with luminosity from the HII galaxies to the SBNs.

Most of the compact galaxies in the intermediate sample lie in the moderate to high-excitation regime populated by local HII galaxies and moderate- $z$  CNELGs (i.e.,  $\log [\text{OIII}]/\text{H}\beta > 0.3$ ). Direct comparison with Dopita & Evans (1986) models yields an average metallicity  $Z \sim 0.4Z_{\odot}$  for compact galaxies in this excitation regime. This value is consistent with that derived from the luminosity–metallicity relation for local emission-line galaxies in the same range of luminosities (Salzer *et al.* 1989). A few objects have low  $[\text{OIII}]/\text{H}\beta$  ratios consistent with more evolved star-forming systems such as local DANS and SBNs (hereafter called ‘starburst disk galaxies’). The average metallicities for these objects are  $Z \sim 0.8Z_{\odot}$ . From the analysis of  $[\text{OIII}]/\text{H}\beta$  vs.  $M_B$ , we conclude that emission-line compact objects at  $z < 0.7$  are vigorously star-forming galaxies covering a broad range in metallicity.

#### 4.2. The $\text{H}\beta$ Luminosity vs. Velocity Width Diagram

For star-forming galaxies with a dominant young population, the flux of the Balmer lines provide a reliable estimate of the age and the strength of the on-going burst (Dopita & Evans 1986; Mas-Hesse & Kunth 1991; Leitherer & Heckman 1995). A useful diagram to study intrinsic differences in the evolutionary state of various types of star-forming galaxies is  $\text{H}\beta$  luminosity vs. velocity width since the starburst properties can be compared among galaxies with similar internal kinematics, i.e., independently of any luminosity evolution. Figure 4 shows the  $L_{\text{H}\beta} - \sigma$  diagram for the 28 compact galaxies with reliable  $L_{\text{H}\beta}$  measurements. Only 4 of these objects have  $z > 0.7$  (filled squares). For comparison, we also show the sample of local HII galaxies studied by Melnick, Terlevich & Moles (1988), as well as the sample of CNELGs with  $\sigma < 70 \text{ km s}^{-1}$  presented in Koo *et al.* (1995). Since  $L_{\text{H}\beta}$  measurements for both compact galaxies and CNELGs have not been corrected for internal extinction, we have decreased the corrected  $L_{\text{H}\beta}$  values of local HII galaxies by

$\sim 0.7$  dex, which corresponds to the average value of the extinction correction for luminous HII galaxies (Gallego *et al.* 1997). We also plot a sample of local infrared-selected starburst disk galaxies studied by Lehnert & Heckman (1996).  $H\beta$  luminosities were derived from extinction-corrected  $H\alpha$  luminosities, i.e.  $L_{H\beta} = L_{H\alpha}/2.86$ . These values were decreased by 0.9 dex to account for the average extinction correction applied to starburst disk galaxies (Gallego *et al.* 1997). Velocity widths were derived from their rotational velocity measurements, assuming  $\sigma = 0.426 \times 2V_{rot}/\sin i$ .

In the  $L_{H\beta} - \sigma$  diagram, HII galaxies with  $EW_{H\beta} > 30\text{\AA}$  follow a well-defined correlation:  $L_{H\beta} \propto \sigma^5$  (Terlevich & Melnick 1981). CNELGs also follow the same trend (Koo *et al.* 1995), while starburst disk galaxies define a similar relation that is offset towards lower  $L_{H\beta}$  by a factor of  $\sim 30$  at a given  $\sigma$ . The distributions of local HII galaxies and starburst disk systems define the boundaries for the overall observed range in  $L_{H\beta}$  at any given  $\sigma$  of compact galaxies. The large observed spread in  $L_{H\beta}$  reflects variations in metallicity (Terlevich & Melnick 1981), extinction (since no corrections have been applied), and strength of the current burst of star formation (since the luminosity of the Balmer lines scales directly with the SFR). Differences in the relative contribution of turbulent and virial motions to the velocity widths in our sample galaxies may also affect their distribution in Figure 4, although the effect seems to be noticeable mainly in objects with  $\sigma > 60 \text{ km s}^{-1}$  (Melnick, Terlevich & Moles 1988). On average at a given  $\sigma$ , low  $L_{H\beta}$  compact galaxies tend to have  $\sim 50\%$  lower excitation (i.e., higher metallicity) and  $\sim 6$  times lower SFRs than their counterparts with high  $L_{H\beta}$ .

Roughly, half of the compact galaxies shown in this diagram have  $H\beta$  luminosities and velocity widths similar to those of extreme star-forming HII galaxies, in agreement with the analysis of the line-ratio diagram discussed previously. This can be interpreted as the result of having average metallicity, extinction, and SFR consistent with those values

typical for HII galaxies. The remaining have  $L_{H\beta}$  and  $\sigma$  values indicative of being more evolved star-forming systems with metallicity, extinction, and SFR approaching values characteristic of local starburst disk galaxies.

### 4.3. The [OII] Equivalent Width vs. Luminosity Diagram

The [OII] luminosity ( $L_{[OII]}$ ) is a good tracer of the SFR (Gallagher *et al.* 1989; Kennicutt 1992). In the absence of flux-calibrated spectra,  $L_{[OII]}$  can be estimated using [OII] equivalent widths and blue luminosities (i.e.,  $L_{[OII]} \sim 10^{29} EW_{[OII]} L_B$ ; see Appendix). The  $EW_{[OII]} - M_B$  diagram thus provides direct information on the star formation activity. Figure 5 shows the  $EW_{[OII]} - M_B$  diagram for the whole sample of distant compact objects, as well as for a representative sample of local emission-line galaxies (Salzer *et al.* 1989; Gallego *et al.* 1997). The [OII] emission lines of compact galaxies are remarkably strong (equivalent widths of  $\sim 60\text{\AA}$  in the integrated spectrum), given that these are luminous galaxies with absolute  $B$  magnitudes of about  $-20$ . In agreement with the results derived in the previous sections, compact galaxies in the intermediate- $z$  sample show [OII] equivalent widths and blue luminosities consistent with those values characteristic of local HII and starburst disk galaxies. In particular, compact galaxies with high excitation and high  $L_{H\beta}$  at a given  $\sigma$  tend to have large  $EW_{[OII]}$  similar to HII galaxies. High- $z$  compacts also show [OII] equivalent widths and blue luminosities that overlap the observed distribution for local vigorously star-forming galaxies. However, although high- $z$  compacts exhibit a similar range in  $EW_{[OII]}$  to that of compacts at intermediate- $z$ , they are  $\sim 1$ - $2$  mag brighter. This implies that, on average at the same equivalent width, compact galaxies at  $z > 0.7$  have higher [OII] luminosities by a factor  $\sim 10$  than those at  $z < 0.7$ , which in turn translates into their having  $\sim 10$  times higher SFR.

The increase in the [OII] luminosity with redshift suggests an enhancement of the



SFR in compact galaxies at higher redshifts. To assess whether this enhancement implies a significant evolution in the star formation activity of compact galaxies, it is necessary to take into account the selection effects at play in our sample. Because of the cutoffs in  $r_{1/2}$ ,  $I_{814}$  and  $\mu_{I814}$  applied, the global galaxy properties of our sample are strongly correlated with redshift, and also among each other. This is clearly shown in Figure 6, where we plot the distribution of  $L_{[OII]}$  (or SFR) as a function of surface brightness for the intermediate- and high- $z$  samples. Superimposed on the data points, we plot the approximate limits of the observable window defined by our selection effects at  $z \sim 0.55$  (i.e.,  $1.3 < R_e < 4$  kpc,  $M_B < -18.25$ , and  $SB_e < 22.0$ ), and at  $z \sim 0.85$  (i.e.,  $1.6 < R_e < 5$  kpc,  $M_B < -19.25$ , and  $SB_e < 21.2$ ). These are, in fact, the same boundaries described in Paper I using the  $M_B - SB_e$  diagram. Figure 6 demonstrates that selection effects can account for the lack of compact galaxies with low  $L_{[OII]}$  in the high- $z$  sample. However, they cannot explain why compacts with  $L_{[OII]} \geq 10^{41}$  erg s $^{-1}$  are so rare in the intermediate- $z$  sample. The shaded region defined by the intersection of both observable windows represents the area of the parameter space available to our sample galaxies in the redshift range  $0.4 < z < 1$ , approximately. If the apparent lack of high  $L_{[OII]}$  systems in the intermediate- $z$  sample were due to selection effects, then high- and intermediate- $z$  compacts within the shaded region would show a *similar* distribution. However, the segregation in  $L_{[OII]}$  between the two samples still remains. Note that the volumes mapped at  $0.4 < z < 0.7$  and  $0.7 < z < 1$  are comparable (i.e.,  $1.6 \times 10^4$  Mpc $^3$  and  $2.3 \times 10^4$  Mpc $^3$ , respectively), so a volume-richness effect is not present. The sparsity of high  $L_{[OII]}$  compacts in the intermediate- $z$  sample, as compared to the numbers observed at  $z > 0.7$ , points towards a steep evolution of the star formation activity in compact galaxies with redshift. Given the small number of objects involved, however, it is difficult to demonstrate with our sample that significant evolution has actually occurred.

Previous surveys (Glazebrook *et al.* 1995; Cowie *et al.* 1995) have pointed to the

presence of vigorously star-forming galaxies at  $z \sim 1$ . These galaxies have unusually high [OII] luminosities ( $L_{[\text{OII}]} \sim 10^{42}$  erg s $^{-1}$ ) that are rarely seen in field galaxy samples at  $z < 0.7$  and locally. HST observations for nine such galaxies show compact objects with complicated morphologies such as chains and compact blobs (Cowie *et al.* 1995). Spectroscopically, they show very strong [OII] emission lines and several absorption features identified as MgII, MgI and FeII. These objects are similar in their structural and spectroscopic properties to the subset of seven extreme star-forming compact galaxies at  $z > 0.7$  mentioned in Section 2. High- $z$  compact galaxies, however, do resemble nearby vigorously star-forming systems in terms of [OII] equivalent widths and blue luminosities (Figure 5). This suggests that the more distant compact galaxies are not necessarily in unique evolutionary states, but may simply be larger versions of the same starburst systems observed at lower redshifts.

#### 4.4. The specific SFR vs. Mass Diagram

To quantify the starburst nature of the compact galaxy sample, we introduce a new parameter: the SFR per unit mass (or *specific* SFR), which reflects the strength of the current burst of star formation relative to the underlying galaxy mass. Masses can be estimated via the virial theorem using the half-light radius and velocity width as a measure of the galaxy size and gravitational potential. For star-forming galaxies, the virial masses will very likely underestimate the total mass, depending on galaxy type, inclination and aperture effects, and the presence of any older, extended stellar population (e.g., see Guzmán *et al.* 1996). This may introduce a bias in the comparison of the specific SFRs derived for various galaxy types. A detailed discussion on the reliability of virial mass estimates for our compact galaxy sample is presented in Paper I. For the purposes of this paper, we have made an independent assessment of this bias by comparing the specific

SFR derived using total and virial masses for a sample of 12 nearby blue galaxies with  $-22 < M_B < -15$  that best resembles the characteristics of our compact sample. The total mass in gas and stars for a galaxy can be estimated from the measured HI mass and optical luminosity (i.e.,  $M_{total} \sim 1.34 M_{HI} + \left(\frac{M_*}{L_*}\right) L_B$ ; Hunter & Gallagher 1986). Using the values for  $SFR/M_{total}$  listed in Table 2 of Hunter & Gallagher (1986), as well as published velocity widths (Hunter, Gallagher & Rautenkranz 1982), [OII] equivalent widths (Gallagher *et al.* 1989) and half-light radii (de Vaucouleurs *et al.* 1991), we derive:

$$\frac{SFR/M_{virial}}{SFR/M_{total}} = 1.3 \pm 0.1$$

Since we have used the same calibration for the SFR, this comparison implies that virial masses are underestimating the total masses for this sample of very blue, star-forming galaxies by  $\sim 30\% \pm 15\%$  (i.e., less than a factor  $\sim 2$  at the most). This value does not depend significantly on whether only high- or low-luminosity galaxies are considered in the comparison. We thus conclude that the uncertainty introduced by using virial mass estimates to determine the  $SFR/M$  of blue star-forming systems, such as our compact galaxies, is typically less than a factor  $\sim 2$  over a range of  $\sim 7$  mag in luminosities.

Figure 7 shows the specific SFR (normalized to  $10^{11} M_\odot$ ) versus mass for the whole sample of compact galaxies as well as for the sample of HII galaxies, CNELGs and starburst disk galaxies described in Figure 4. Also for comparison, we include two other samples of nearby blue galaxies (Gallagher *et al.* 1989) and luminous starbursts (Calzetti 1997) with kinematic data. Virial mass estimates for our compact galaxies are listed in Paper I. For HII galaxies, masses were derived using the half-light radius and  $\sigma$  measurements listed in Telles (1995), assuming the same structural constant adopted for our compact objects. The SFRs of HII galaxies were derived using  $L_{H\alpha}$  (see Appendix), assuming  $L_{H\alpha}^{obs} E(L_{H\alpha}) = 2.86 \times L_{H\beta}$ , where  $E(L_{H\alpha})$  is the correction for extinction in  $L_{H\alpha}$ , and  $L_{H\beta}$  are the extinction-corrected luminosities given in Melnick, Terlevich & Moles (1988). For

CNELGs, masses were taken from Guzmán *et al.* (1996), while SFRs were derived from  $EW_{[OII]}$  measurements (Koo, unpublished). Only three such objects have observations of [OII]. Masses and star formation rates for Lehnert & Heckman’s sample of local starburst disk galaxies were derived from their published values of  $R_e$ ,  $V_{rot}/\sin i$  and  $L_{H\alpha}$ , assuming the gas is in dynamical equilibrium with the same potential sensed by the disk gas, and an average extinction correction of  $\sim 0.4$  dex in the observed  $L_{H\alpha}$ . For the blue galaxy sample, we derive masses and SFRs from published velocity widths (Hunter, Gallagher & Rautenkranz 1982), [OII] equivalent widths (Gallagher *et al.* 1989) and half-light radii (de Vaucouleurs *et al.* 1991). Finally, the data for nearby luminous starbursts is taken directly from Calzetti (1997).

The  $SFR/M$  vs  $M$  diagram is particularly useful to analyse the nature of compact galaxies using the star formation activity as the only measure of the evolutionary state of galaxies with the same mass (instead of luminosity, which depends itself on evolution). In this diagram, HII galaxies and CNELGs describe a well-defined sequence showing relatively constant values of the specific SFR at the top of the overall galaxy distribution. The scatter is only  $\sim 0.25$  dex in  $SFR/M$  over two orders of magnitude in mass. Most local starburst disk systems likewise exhibit relatively constant specific SFRs, but at a rate  $\sim 30$  times smaller than that of HII galaxies. These two galaxy types define clear boundaries to the distribution of compact objects. The distribution of compacts in the  $SFR/M - M$  diagram is indeed very similar to that observed in the  $EW_{[OII]} - M_B$  diagram. This supports our assumption that any systematic bias in the mass estimates among compact galaxies is small compared to the intrinsic differences in their star formation activity.

There are two major results that can be directly drawn from Figure 7. First, the highest values of the specific SFR exhibited by compact galaxies are consistent with those characteristic of local HII galaxies. Thus we do not find evidence for an increase in the

peak of the specific SFR activity with redshift in our sample. Second, compact galaxies at  $z > 0.7$  are, on average,  $\sim 10$  times more massive than their counterparts with similar specific SFR at  $z < 0.7$  (or, alternatively, they have  $\sim 10$  higher  $SFR/M$  at a given mass). This effect is partly due to the magnitude cutoff adopted in our sample selection, which translates into an offset in the low-end of the mass distribution for both samples. As shown in Figure 6, this cutoff implies a difference of  $\sim 1$  mag between the absolute blue magnitude limits at  $z \sim 0.55$  and  $z \sim 0.85$ . Assuming similar mass-to-light ratios for compact galaxies in both samples, the above magnitude difference yields an offset of  $\sim 0.4$  dex in the lower limit of the expected mass distributions for the high- and intermediate- $z$  samples, which is consistent with that observed.

Although selection effects may account for the lack of low-mass compact objects at high redshift, they cannot explain why the massive star-forming systems are not present in the intermediate redshift sample. Figure 8 shows the  $SFR/M$  vs  $M$  diagram for the sub-sample of compact galaxies that could have been observed over the whole range of redshifts  $0.4 < z < 1$ , as discussed in Section 4.3. Superimposed on the data points we have plotted the approximate boundaries of the shaded region shown in Figure 6. If the apparent lack of massive star-forming systems at  $z < 0.7$  were due to selection effects, then compact galaxies in the intermediate- and high- $z$  samples should show a similar distribution in this figure. However, despite the small number of data points, the segregation in mass between the two samples is still noticeable. This is the same effect seen in the distribution of [OII] luminosities and described in Section 4.3. The enhancement of the SFR in compact galaxies with redshift suggested by the analysis of  $L_{[OII]}$  is not thus the result of high- $z$  compacts having unusually high star formation activity per unit mass. Rather, compacts at  $z > 0.7$  have similar specific SFR to those at  $z < 0.7$ , but are *intrinsically more massive*. These results agree qualitatively with the “downsizing” scenario discussed by Cowie *et al.* (1996), in which more massive galaxies form at higher redshift. Instead of indicating a

new population of massive star-forming systems, Figure 7 shows that these high- $z$  compact galaxies may be related to local luminous starbursts (such as NGC 4385, NGC 4194, or NGC 1614) which, in some aspects, can also be considered high-luminosity counterparts of less luminous HII galaxies (cf. Stasinska & Leitherer 1996). These results thus suggest an increase in the *number of massive star-forming systems* with redshift. To assess whether significant evolution has actually occurred requires information on the relative numbers of field compact emission-line galaxies as a function of mass in distant and nearby galaxy samples. A preliminary attempt to tackle this issue with the currently available data will be presented in Section 5.

Based on these results, we have classified the compact galaxy sample into two classes. Compacts with  $\log(SFR/M) < 1.25$  (i.e., the lower limit for the observed distribution of nearby HII galaxies) are classified as HII-like galaxies. Compacts with  $SFR/M$  smaller than this value are classified as starburst disk-like galaxies. The average global properties of each class are summarized in Tables 2a and 2b. On average, HII-like compact galaxies have smaller half-light radii, larger  $EW_{[OII]}$ , higher surface brightnesses and SFR's per unit mass, and lower M/L ratios than their starburst disk-like counterparts. Within the same type, however, high- $z$  compact galaxies have, on average, larger radii, higher luminosities, larger velocity widths, and are more massive than those at intermediate redshifts. This is consistent with the idea that they are simply larger versions of the same kind of starburst galaxies found at lower redshifts. This broad classification of compact objects into HII-like and starburst disk-like galaxies is also supported by slight morphological differences seen in HST images. HII-like objects show generally very compact, amorphous morphologies, similar to the local HII galaxies (Telles 1995). Starburst disk-like galaxies instead appear to be more diffuse systems, sometimes with a central condensation. This is the expected appearance of local starburst disk galaxies, such as DANS or SBN, placed at intermediate redshifts.

In summary, distant emission-line compact galaxies are similar to local starburst galaxies. About 60% of our sample have luminosities, excitations, velocity dispersions, half-light radii, surface brightnesses, mass-to-light ratios, [OII] equivalent widths, and specific SFRs consistent with being HII galaxies, while the remaining 40% are more similar to starburst disk galaxies. There is no evidence for unusually high values of the specific SFR in our sample. However, we find that high  $SFR/M$  compact objects at  $z > 0.7$  are  $\sim 10$  times more massive than their lower redshift counterparts. The implications for the evolution of the SFR density of the universe will be discussed in the next section.

## 5. The Evolution of the Star Formation Rate Density with Redshift

One important goal in observational cosmology is to determine the star formation history of the universe, and its variation with galaxy type and environment. Recent advances in this active field include new observational data covering a wide range in redshift and improved models on chemical cosmic evolution. The recent UCM survey by Gallego *et al.* (1995) has determined the first reliable  $H\alpha$  luminosity function for the local universe. The integration over all  $H\alpha$  luminosities yields a total SFR density of  $0.004 M_{\odot}/\text{yr}/\text{Mpc}^3$  (using Salpeter IMF and  $H_0=50 \text{ km s}^{-1} \text{ Mpc}^{-1}$ ). This value is almost identical to the estimate derived by Tinsley & Danly (1980) using colors for field spiral galaxies. Compared to the total mass density of stars, the SFR observed by Gallego *et al.* is high enough to make all the stellar content of galaxies observed by the APM survey (Loveday *et al.* 1992) in about 10 Gyr. However, the luminosity density inferred from the APM sample could be too low by a factor of two (Ellis *et al.* 1996). In that case the average past SFR would need to be twice the currently observed value, which seems consistent with the detection of strongly enhanced star formation in intrinsically faint galaxies at redshifts beyond  $z \sim 0.3$  (Ellis *et al.* 1996; Cowie *et al.* 1995; Lilly *et al.* 1995). These results suggest a peak in the

global SFR at  $z \sim 1-2$  (White 1996). Such a trend has been predicted by models of cosmic evolution using different cosmologies (Kauffmann, Guiderdoni & White 1994; Pei & Fall 1995).

Figure 9 shows a current overall picture of the evolution of the SFR density with redshift. Published estimates were transformed to Salpeter IMF, and  $H_0=50 \text{ km s}^{-1} \text{ Mpc}^{-1}$ ,  $q_0=0.5$  cosmology, which are the values most commonly adopted in the various studies quoted in Figure 9. The open circles at  $z = 0$  are the local values derived for the UCM sample (Gallego *et al.* 1995). The filled triangles at intermediate redshifts are SFR densities for the CFRS as derived from 2800 Å, 4400 Å, and 1  $\mu\text{m}$  continuum luminosities (Lilly *et al.* 1996). The stars represent densities obtained using our own  $L_{[OII]}$ -SFR calibration for the data set of Cowie *et al.* (1995), which is  $\sim 90\%$  complete down to  $I_{AB} < 22.5$ . Note that the value at  $z \sim 1.2$  may be largely affected by incompleteness. As an additional constraint for this epoch, we used the upper limits obtained by Mannucci *et al.* (1996) in their search for primeval galaxies at high redshift. A lower limit density at  $z \sim 3$  is given by the UV luminosities of spectroscopically confirmed galaxies (5 initial objects from Steidel *et al.* 1996 plus 11 new ones from Lowenthal *et al.* 1996). The vertical arrows at redshifts  $z \sim 3.2$  and  $z \sim 4$  are lower limit estimates from Madau *et al.* (1996) using photometric redshifts for HDF. The long-dashed horizontal line depicts the fiducial density given by the average luminosity density observed today (Madau *et al.* 1996) translated to mass and divided by the present age of the universe. Finally, we also plot the Pei & Fall (1995) model predictions for three different scenarios: closed-box (C), inflow of metal-free gas (I), and outflow of metal-enriched gas (O).

The interpretation of Figure 9 should be approached with caution, given the likely differences in the calibrations for the various SFR tracers, incompleteness of the data sets, and uncertainties in the models. Despite these caveats, most of the results summarized in



this figure point to a consistent result: the total SFR density of the universe decreased by a factor of  $\sim 10$  from  $z = 1$  to the present-day. The nature of the galaxies responsible for this enhancement of the SFR density with look-back time remains an important unanswered question.

Although incomplete, our sample is still useful to constrain the role of compact galaxies on the evolution of the SFR density at redshifts  $z < 1$ . Instead of computing the SFR density extended to the whole volume covered, we restrict our analysis to two well-sampled regions in redshift space. The first one is centered at  $z = 0.55$ , with redshifts in the range  $z = 0.4$  to  $0.7$  ( $N=22$  objects). The second one is centered at  $z = 0.85$  and ranges from  $z = 0.7$  to  $1.0$  ( $N=16$  objects). For comparison with previous studies, we adopt  $q_0 = 0.5$ . Using the expression obtained in Section 3.2, a straightforward summation of the observed [OII] luminosity within each redshift interval yields co-moving SFR densities of  $0.001 M_{\odot} \text{ yr}^{-1} \text{ Mpc}^{-3}$  at  $z=0.55$ , and  $0.002 M_{\odot} \text{ yr}^{-1} \text{ Mpc}^{-3}$  at  $z=0.85$ . These values correspond to 25% and 50% of the local estimate, respectively. Note, however, that only 63 of a total of  $\sim 245$  (i.e., 25%) initial candidates were actually observed (see Paper I). Assuming our sample is representative of the general population of compact galaxies, we estimate that the total SFR densities associated to this class are:  $0.004 M_{\odot} \text{ yr}^{-1} \text{ Mpc}^{-3}$  at  $z=0.55$ , and  $0.008 M_{\odot} \text{ yr}^{-1} \text{ Mpc}^{-3}$  at  $z=0.85$ . These values are plotted as filled circles in Figure 9.

A meaningful comparison of the SFR density derived for distant compact galaxies with that of the local universe requires an estimate of the amount of SFR for a *similar* sample of nearby compact galaxies. The point at  $z = 0$  labelled as ‘Interm- $z$ ’ in Figure 9 corresponds to the local SFR density derived using only 19 UCM galaxies that satisfy the same cutoffs in  $M_B$ ,  $SB_e$ , and  $R_e$  applied to compact galaxies at  $z \sim 0.55$  (see Section 4.3). The point at  $z = 0$  labelled as ‘High- $z$ ’ corresponds to the local SFR density derived for only 2 UCM galaxies that satisfy the selection cutoffs at  $z \sim 0.85$ . Given this small number, we will

not consider the high- $z$  compact galaxies in our analysis. Direct comparison between the SFR densities derived for similar samples of nearby and intermediate- $z$  compact galaxies implies an enhancement of a factor  $\sim 10$  in the star formation history of the universe from  $z \sim 0$  to  $z \sim 0.55$ . However, this result should be considered with caution, given the small number of galaxies involved.

The SFR densities derived for compact galaxies can also be compared to the values derived for more complete galaxy samples at similar redshifts. To avoid systematic differences due to the calibration of the SFR using other tracers, we chose those values derived using the  $EW_{[OII]}$  data of Cowie *et al.* as the reference SFR density. According to Figure 5, the global SFR density for star-forming galaxies at  $0.4 < z < 1$  is  $0.022 \text{ M}_{\odot} \text{ yr}^{-1} \text{ Mpc}^{-3}$ . The Cowie *et al.* data refer only to field galaxies with  $I_{AB} < 22.5$ . For comparison, we adopt a similar magnitude limit in our analysis. There are 301 galaxies with  $I_{AB} < 22.5$  in the flanking fields of HDF. The number of compact galaxies in this sample is 102, of which we have observed 21. Since only 14 of these compact galaxies are emission-line systems, we estimate that the fraction of emission-line compact galaxies is  $\sim 20\%$  of the general field galaxy population. Of the 14 emission-line compact galaxies, only 12 are at  $0.4 < z < 1$ . The SFR density for this subsample is  $0.01 \text{ M}_{\odot} \text{ yr}^{-1} \text{ Mpc}^{-3}$ . Thus, we conclude that emission-line compact galaxies, though only  $\sim 20\%$  of the general field population, contribute about  $\sim 45\%$  to the global SFR density at  $0.4 < z < 1$ . This supports an evolutionary scenario where compact galaxies experience major evolution at moderate redshifts. Larger, homogeneous data sets, that include a wide variety of structural, kinematical, and stellar population properties for faint field galaxies, are needed to confirm the important role that compact stellar systems may have in the star formation history of the universe at  $z \leq 1$ .

## 6. Conclusions

We have studied the spectroscopic properties of a representative sample of 51 compact galaxies to  $z < 1.4$  and  $I_{814} < 23.74$  in the flanking fields of the HDF. The main results of this paper can be summarized as follows:

- (i) 88% of the spectra exhibit narrow emission-lines while the remaining 12% have only absorption lines.
- (ii) Emission-line profiles are roughly Gaussian with velocity profiles that range from  $\sigma \sim 35 \text{ km s}^{-1}$  (the measurement limit) to  $150 \text{ km s}^{-1}$ . Rest-frame [OII] $\lambda 3727$  equivalent widths range from  $5\text{\AA}$  to  $94\text{\AA}$ , yielding star formation rates of  $\sim 0.1$  to  $14 \text{ M}_{\odot} \text{ yr}^{-1}$ .
- (iii) Emission-line compact galaxies are very similar to local starburst galaxies. About 60% have velocity widths, excitations,  $H\beta$  luminosities, and star formation rates characteristic of young star-forming HII galaxies. The remaining 40% form a heterogeneous class of more evolved starburst disk galaxies.
- (iv) The distribution of specific SFRs in emission-line compact galaxies at  $z < 0.7$  is very similar to that observed at  $z > 0.7$ . The highest values of specific SFR derived for our sample are consistent with those characteristic of local HII galaxies. Thus we do not find evidence for an enhancement of the specific SFR activity with redshift.
- (v) On average at a given value of the specific SFR, emission-line compact galaxies at  $z > 0.7$  are  $\sim 10$  times more massive than their intermediate- $z$  counterparts. This result supports a general evolutionary scenario in which the SFR density of the universe declines by a factor  $\sim 10$  from  $z \sim 1$  to the present-day.
- (vi) Emission-line compact galaxies account for only  $\sim 20\%$  of the general field galaxy

population with  $I_{AB} < 22.5$  but contribute  $\sim 45\%$  to the total SFR density at  $0.4 < z < 1$ . We conclude that compact galaxies play a significant role in the evolution of the star formation history of the universe at moderate redshifts.

We thank Caryl Gronwall for providing the model SEDs used for  $k$ -corrections and Katherine Wu for useful comments. We are grateful to the staff of the W.M. Keck Observatory for their help during the observations. We also thank Gregory Bothun and an anonymous referee for helpful comments which contributed to improve the quality of this paper. Funding for this work was provided by NASA grants AR-06337.08-94A, AR-06337.21-94A, GO-05994.01-94A, AR-5801.01-94A, and AR-6402.01-95A from the Space Telescope Institute, which is operated by AURA, Inc., under NASA contract NAS5-26555. We also acknowledge support by NSF grants AST 91-20005 and AST 95-29098. JG acknowledges the partial financial support from Spanish MEC grants PB89-124 and PB93-456 and a UCM del Amo foundation fellowship. JDL acknowledges funding from the Hubble Fellowship grant HF-1048.01-93A. This research has made use of the NASA/IPAC Extragalactic Database (NED) which is operated by the Jet Propulsion Laboratory, Caltech, under contract with NASA.

## 6.1. Appendix

Although the nebular  $H\alpha$  luminosity is among the best direct measurements of the current SFR (modulo the IMF), this emission line is visible in the optical ( $\lambda < 0.9\mu$ ) out to only  $z \sim 0.4$ . At higher redshifts, the main indicators used for estimating the SFR are diverse: [OII]  $\lambda 3727$  luminosity (Dressler & Gunn 1982; Gallagher *et al.* 1984, 1989; Broadhurst *et al.* 1992; Kennicutt 1992; Cowie *et al.* 1995; Ellis *et al.* 1996), continuum colors (Tinsley & Danly 1980; Lilly *et al.* 1996) and rest-frame UV luminosities

(Steidel *et al.* 1996; Madau *et al.* 1996; Lowenthal *et al.* 1996). Since most emission-line compact galaxies have reliable  $EW_{[OII]}$  measurements, we chose to characterize their star formation activity using  $EW_{[OII]}$ . In order to estimate the SFR, we have derived our own transformation between  $H\alpha$  luminosity and  $EW_{[OII]}$  using a sample of local emission-line galaxies that best resembles the characteristics of compact galaxies. Figure 10 shows the  $\log(EW_{[OII]}/EW_{[OIII]})$  vs.  $\log([OIII]/H\beta)$  diagram for galaxies in the intermediate compact sample compared to a representative sample of starburst galaxies from Terlevich *et al.* (1991). Most of our objects have  $\log(EW_{[OII]}/EW_{[OIII]}) > -0.25$ . Thus, as a control sample, we considered only those local galaxies that satisfy the above condition. With this local sample of 136 objects, we follow a similar procedure to that described by Kennicutt (1992). Assuming a standard Salpeter IMF with  $m_L=0.1 M_\odot$  and  $m_U=125 M_\odot$ , the SFR is related to the observed  $H\alpha$  luminosity by the expression (Alonso-Herrero *et al.* 1996):

$$SFR(M_\odot yr^{-1}) = 3.2 \times 10^{-42} L_{H\alpha}^{obs} E_{H\alpha}$$

where  $E(H\alpha)$  is the extinction correction in the  $H\alpha$  luminosity as derived from the Balmer decrement. Note that the coefficient of the new relation is  $\sim 3$  times smaller than that derived by Kennicutt. This difference is largely due to the use of a different IMF (Alonso-Herrero *et al.* 1996). Thus, in terms of the observed  $[OII]$  luminosity:

$$SFR(M_\odot yr^{-1}) = 3.2 \times 10^{-42} \left( \frac{L_{H\alpha}}{L_{[OII]}} \right)_{obs} L_{[OII]}^{obs} E_{H\alpha}$$

For the local sample:

$$\left\langle \left( \frac{L_{H\alpha}}{L_{[OII]}} \right)_{obs} \times E_{H\alpha} \right\rangle = 7.42 \pm 1.23$$

Adopting the average value as representative for this type of galaxy:

$$SFR(M_{\odot}yr^{-1}) = 2.4 \times 10^{-41} L_{[OII]}$$

The above coefficient is  $\sim 2$  times smaller than the average calibration derived by Kennicutt for spiral galaxies. For very blue galaxies, however, such as those in our control sample and in the compact galaxy sample, his estimates are expected to be as much as a factor of three lower (Kennicutt 1992), which is consistent with our value. Finally, we derive the transformation between [OII] luminosity and  $EW_{[OII]}$  using a subsample of 75 galaxies in the control sample with known absolute blue magnitudes, [OII] fluxes, and  $EW_{[OII]}$  (Terlevich *et al.* 1991). The least-squares fit to the data yields:

$$\frac{L_{[OII]}}{EW_{[OII]}} = 1.03 \pm 0.11 \times 10^{29} L_B(L_{\odot})$$

This relation is linear over the whole range in absolute magnitude exhibited by our control sample (i.e.,  $-21 < M_B < -16$ ). Substituting  $L_{[OII]}$  according to this relation, the general expression to estimate SFR as a function of the observed  $EW_{[OII]}$  is:

$$SFR(M_{\odot} yr^{-1}) \approx 2.5 \times 10^{-12} \times 10^{-0.4(M_B - M_{B\odot})} EW_{[OII]}$$

Note that the above calibration may not apply for compact objects with extreme ionization (i.e.,  $\log(EW_{[OII]}/EW_{[OIII]}) < -0.5$ ). There are two such objects in our sample: sw3\_1455\_0476 is a nearby low-luminosity blue compact dwarf with a very high excitation ( $EW_{[OII]}/EW_{[OIII]}=0.26$ ,  $[OIII]/H\beta=5.27$ ). The emission lines reveal a low-metallicity object where the electronic temperature is very high and most of the oxygen atoms are  $O^{++}$ . In such situations, the SFR derived from the [OII] luminosity may be seriously underestimated. Since  $H\alpha$  is still visible for this object, we were able to obtain a direct measurement of the SFR from  $H\alpha$ . Using [OII] we derived a  $SFR=0.2 M_{\odot}/yr$

while  $H\alpha$  yields  $1.2 M_{\odot}/\text{yr}$ . We adopt the latter value as correct. The same situation applies to ie3\_1030\_0507 ( $\text{EW}[\text{OII}]/\text{EW}[\text{OIII}]=0.215$ ,  $[\text{OIII}]/H\beta=5.42$ ). In this case, the EW[OII]-based SFR quoted in Table 1 may be underestimated by as much as a factor of five.

## REFERENCES

- Alonso-Herrero, A., Aragón-Salamanca, A., Zamorano, J., & Rego, M. 1996, MNRAS, 278, 417
- Babul, A., & Ferguson, H. C. 1996, ApJ, 458, 100
- Baldwin, J. A., Phillips, M. M., & Terlevich, R. 1981, PASP, 93, 5
- Broadhurst, T. J., Ellis, R. S., & Glazebrook, K. 1992, Nature, 355, 55
- Calzetti D., 1997, AJ, in press
- Cole, S., Ellis, R. S., Broadhurst, T. J., & Colless, M. M. 1994, MNRAS, 267, 541
- Colless, M. M., Ellis, R. S., Taylor, K., & Hook, R. N. 1990, MNRAS, 244, 408
- Cowie, L. L., Songaila, A., & Hu, E. M. 1991, Nature, 354, 460
- Cowie, L. L., Hu, E. M., & Songaila, A. 1995, Nature, 377, 603
- Cowie, L. L., Songaila, A., Hu, E. M., & Cohen J. 1996, AJ, 112, 839
- de Vaucouleurs G., de Vaucouleurs A., Corwing, H. G., Buta, R. J., Paturel G. & Fouqué P. 1991, Third Reference Catalog of Bright Galaxies, (Springer-Verlag)
- Dopita, M. A., & Evans, I. N. 1986, ApJ, 307, 431
- Dressler, A., & Gunn J. E. 1982, ApJ, 263, 533
- Ellis, R. 1996, in ESO Workshop on *The Early Universe with the VLT*, 1-4 April, Munich
- Ellis, R. S., Colless, M. M., Broadhurst, T. J., Heyl, J. S., & Glazebrook, K. 1996, MNRAS, 280, 235
- Forbes, D., Phillips, A. C., Koo, D. C., & Illingworth, G. D. 1996, ApJ, 462, 89
- Gallagher, J. S., Hunter, D. A., & Tutukov, A. V. 1984, ApJ, 284, 544
- Gallagher, J. S., Hunter, D. A., & Bushouse, H. 1989, AJ, 98, 806



- Gallego, J., Zamorano, J., Aragón-Salamanca, A., & Rego, M. 1995, ApJ, 455, L1
- Gallego, J., Zamorano, J., Rego, M., & Vitores, A. G. 1997, ApJ, in press
- Glazebrook, K., Ellis, R. S., Colless, M. M., Broadhurst, T. J., Allington-Smith, J. R., & Tanvir, N. R. 1995, MNRAS, 273, 157
- Guiderdoni, B., & Rocca-Volmerange, B. 1990, A&A, 227, 362
- Guzmán, R., Koo, D. C., Faber, S. M., Illingworth, G. D., Takamiya, M., Kron, R., & Bershady, M. A. 1996, ApJ, 460, L5
- Hunter, D. A., & Gallagher, J. S., 1986, PASP, 98, 5
- Hunter, D. A., Gallagher, J. S., & Rautenkranz D., 1982, ApJS, 49, 53
- Kauffmann, G., & White, S. D. M. 1993, MNRAS, 261, 921
- Kauffmann, G., Guiderdoni, B., & White, S. D. M. 1994, MNRAS, 267, 981
- Kennicutt, R. C. 1992, ApJ, 388, 310
- Kennicutt, R. C., Tamblyn, P., & Congdon, C. E. 1994, ApJ, 435, 22
- Kinney, A. L., Bohlin, R. C., Calzetti, D., Panagia, N., & Wyse, R. F. G., 1996, preprint
- Koo, D. C., & Kron, R. 1992, ARA&A, 30, 613
- Koo, D. C., Guzmán, R., Faber, S. M., Illingworth, G. D., Bershady, M. A., Kron, R. G., & Takamiya, M. 1995, ApJ, 440, L49
- Koo, D. C. 1995, in *Wide Field Spectroscopy & the Distant Universe*, eds. S. Maddox & A. Aragón-Salamanca (Singapore: World Scientific), 55
- Lehnert, M. D., & Heckman, T. M. 1996, ApJ, 462, 651
- Leitherer, C., & Heckman, T. M. 1995, ApJS, 96, 9
- Lilly, S. J. 1993, ApJ, 411, 501
- Lilly, S. J., Tresse, L., Hammer, F., Crampton, D., & Le Fevre, O. 1995, ApJ, 455, L108

- Lilly, S. J., Le Fevre, O., Hammer, F., & Crampton, D. 1996, ApJ, 460, L1
- Loveday, J., Peterson, B. A., Efstathiou, G., & Maddox, S. J. 1992, ApJ, 390, 338
- Lowenthal, J. D., Koo, D. C., Guzmán, R., Gallego, J., Phillips, A. C., Faber, S. M., Vogt, N. P., & Illingworth, G. D. 1996, ApJ, in press
- Madau, P., Ferguson, H. C., Dickinson, M. E., Giavalisco, M., Steidel, C. C., & Fruchter, A. 1996, MNRAS, in press
- Mannucci, F., Thompson, D., & Beckwith, S. V. W. 1996, in *HST and the High Redshift Universe*, 7th Herstmonceux Conf., Cambridge UK, 1-5 July 1996,
- Mas-Hesse, J. M., & Kunth, D. 1991, A&AS, 88, 399
- Melnick, J., Terlevich, R., & Moles, M. 1988, MNRAS, 235, 297
- Morgan, W. W. 1958, AJ, 63, 180
- Oke, J. B., *et al.* 1995, PASP, 107, 375
- Pei, Y. C., & Fall, S. M. 1995, ApJ, 454, 69
- Phillipps, S., & Driver, S. 1995, MNRAS, 274, 832
- Phillips, A. C., Guzmán, R., Gallego, J., Koo, D. C., Lowenthal, J. D., Vogt, N. P., Faber, S. M., & Illingworth, G. D. 1996, ApJ, submitted
- Rix, H.W., Guhathakurta, P., Colless, M., & Ing K. 1997, MNRAS, in press
- Salzer, J. J., MacAlpine, G. M., & Boroson, T. A. 1989, ApJS, 70, 479
- Stasinska, G. 1990, A&AS, 83, 501
- Stasinska, G., Leitherer, C. 1996, ApJ, in press
- Steidel, C. C., & Sargent, W. L. W. 1992, ApJS, 80, 1
- Steidel, C. C., Giavalisco, M., Pettini, M., Dickinson, M., & Adelberger, K. L. 1996, ApJ, 462, L17

- Telles, E. 1995, Ph.D Thesis, IoA, Cambridge
- Tinsley, B. M., & Danly, L. 1980, ApJ, 242, 442
- Tresse, L., Rola, C., Hammer, F., Stasinska, G., Le Fevre, O., Lilly, S. J., & Crampton, D. 1996, MNRAS, in press
- Terlevich, R., & Melnick, J. 1981, MNRAS, 195, 389
- Terlevich, R., Melnick, J., Masegosa, J., Moles, M., & Copetti, M. V. F. 1991, A&AS, 91, 285
- Tinsley, B. M., & Danly, L. 1980, ApJ, 242, 435
- Veilleux, S., & Osterbrock, D. E. 1987, ApJS, 63, 295
- Vogt, N. P., Phillips, A. C., Faber, S. M., Gallego, J., Gronwall, C., Guzmán, R., Illingworth, G. D., Koo, D. C., & Lowenthal, J. D. 1996, ApJ, in press
- Vogt, N.P., *et al.* 1996, ApJ, submitted
- White, S. D. M. 1996, in *Proceedings of the ESO workshop on Large Millimeter Arrays*, ed. P. Shaver,
- Williams R.,E., *et al.* 1996, AJ, 112, 1335

### Figure Captions

Fig. 1.— Spectra of five objects showing a wide range of spectroscopic properties: (a) absorption spectrum characteristic of early-type galaxies; (b) emission-line spectrum characteristic of low-excitation HII regions; (c) emission-line spectrum characteristic of high-excitation HII regions; (d) emission-line spectrum with strong blue continuum and FeII and MgII absorption features similar to that of starbursts undergoing a violent episode of star formation; (e) emission-line spectrum with narrow MgII in emission.

Fig. 2.— Histograms of emission-line measurements for the intermediate- and high- $z$  samples of compact galaxies: (a) [OII] equivalent widths; (b) velocity widths. A significant fraction of objects have  $\sigma$  upper-limits of  $35 \text{ km s}^{-1}$  (hatched region), which corresponds to the measurement limit; (c) star formation rates.

Fig. 3.— Rest-frame absolute blue magnitude versus excitation for the intermediate sample (open squares). Only one object from the high- $z$  sample has measurable [OIII]/ $H\beta$  ratio (filled square). The local sample is represented by the  $H\alpha$ -selected emission-line galaxies analyzed by Gallego *et al.* (1997), and includes Seyfert-2 galaxies (Sy 2), HII galaxies (HII), starburst nuclei (SBN), and dwarf amorphous nuclei starbursts (DANS). Symbols are as explained in the legend. A sample of compact, narrow emission-line galaxies (CNELGs) at  $z = 0.1 - 0.7$  (Koo *et al.* 1995; Guzmán *et al.* 1996) is also shown (stars). The location of more quiescent, early-type spirals is represented by the box.

Fig. 4.— Velocity width  $\sigma$  in  $\text{km s}^{-1}$  versus observed  $H\beta$  luminosity in  $\text{erg s}^{-1}$ . Symbols for the compact objects are as in Fig 3. Infrared-selected starbursts disk galaxies (Lehnert & Heckman 1996) are plotted as ‘ $\oplus$ ’. The arrows represent upper-limit  $\sigma$  measurements. The approximate location of spiral galaxies is represented by the box. The error bar is an estimate of the uncertainty associated to the extinction corrections characteristic of the

various galaxy types plotted in this figure.

Fig. 5.— Rest-frame absolute blue magnitude versus [OII] equivalent width for our sample of compact galaxies as well as a representative sample of nearby emission-line galaxies. Symbols are as in Figure 3.

Fig. 6.— Rest-frame average blue surface brightness in  $\text{mag arcsec}^{-2}$  versus [OII] luminosity in  $\text{erg s}^{-1}$  for our sample of compact galaxies. Symbols are as in Figure 3. Dashed lines represent the observable window in parameter space defined by the selection effects at  $z \sim 0.55$  as described in section 4.3. Dotted lines represent the same observable window at  $z \sim 0.85$ . The shaded area corresponds to the intersection of both windows and represents approximately the region of the parameter space that is available for observation over the redshift range  $0.4 < z < 1$ , as defined by the selection effects.

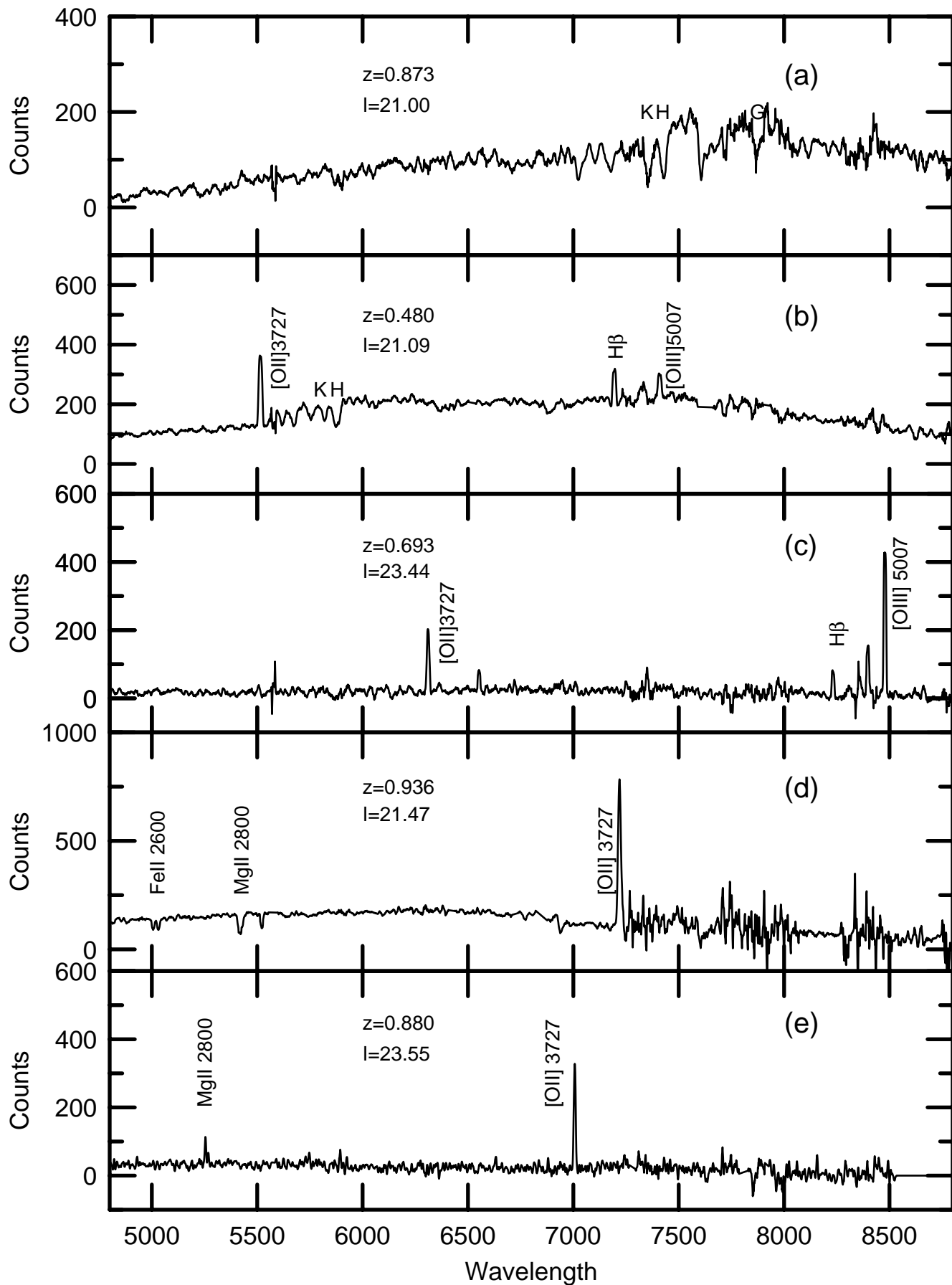
Fig. 7.— Mass in  $M_{\odot}$  versus star formation rate per unit mass in  $\text{yr}^{-1}$  (normalized to  $10^{11}M_{\odot}$ ). Symbols are as in Figure 4. Samples of nearby Irr galaxies (Gallagher *et al.* 1989) and luminous starbursts (Calzetti 1997) are also plotted. The arrows represent upper-limits in  $M$  and lower-limits in  $SFR/M$  due to our measurement limit in  $\sigma$ . The dotted line shows the division between HII-like and starburst disk-like galaxy types as discussed in section 4.4.

Fig. 8.— Mass in  $M_{\odot}$  versus star formation rate per unit mass in  $\text{yr}^{-1}$  (normalized to  $10^{11}M_{\odot}$ ) for a sub-sample of compact galaxies within the shaded area shown in Figure 6. This sub-sample corresponds to those galaxies that could have been observed over the entire redshift range  $0.4 < z < 1$ , as discussed in section 4.3. Solid lines represent approximately the limits defined by our selection effects. Note the segregation in mass between the intermediate- and high- $z$  samples.

Fig. 9.— Current SFR density as a function of redshift (assuming Salpeter IMF and  $H_0=50$

km s<sup>-1</sup> Mpc<sup>-1</sup>, q<sub>0</sub>=0.5 cosmology). The horizontal dashed line represents the value needed to produce the observed stars today. The dotted lines represent Pei & Fall's (1995) predictions: C = Closed-box model, I = Inflow of metal-free gas model, and O = Outflow of metal-enriched gas model. See text in Section 5 for description of the various data sets.

Fig. 10.— Excitation versus [OII]/[OIII] ratio. Open squares are compact objects in the intermediate-*z* sample. Filled squares are compact galaxies in the high-*z* sample. Crosses show the sample of starburst systems from Terlevich *et al*'s (1991) atlas of HII galaxies.



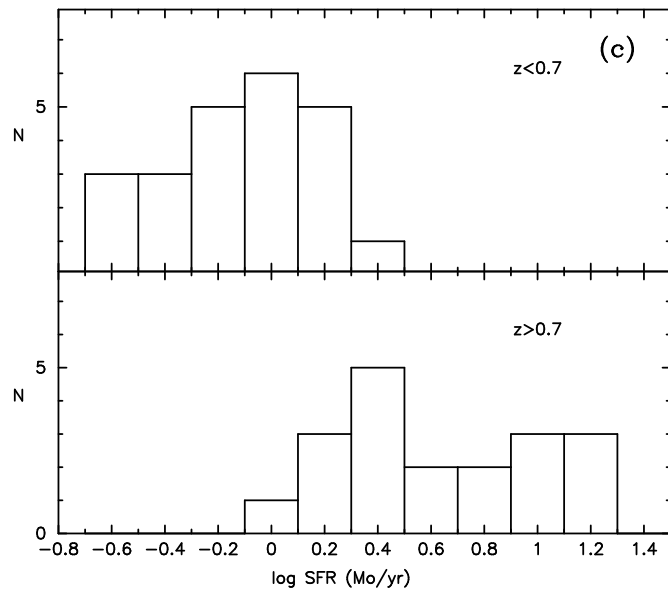
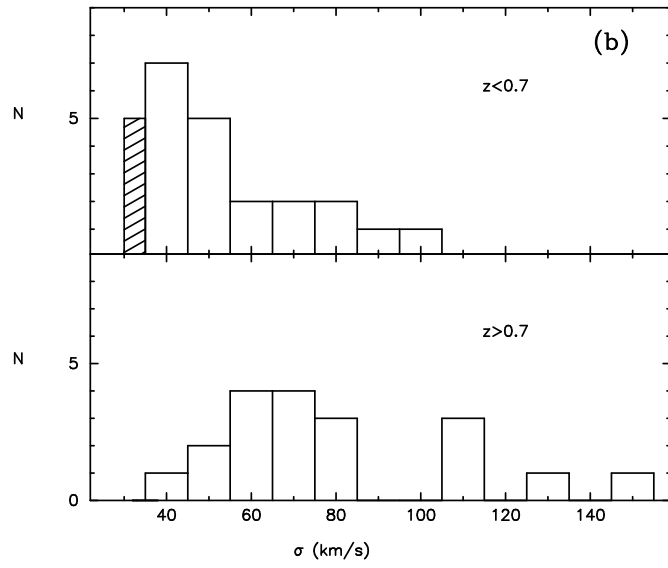
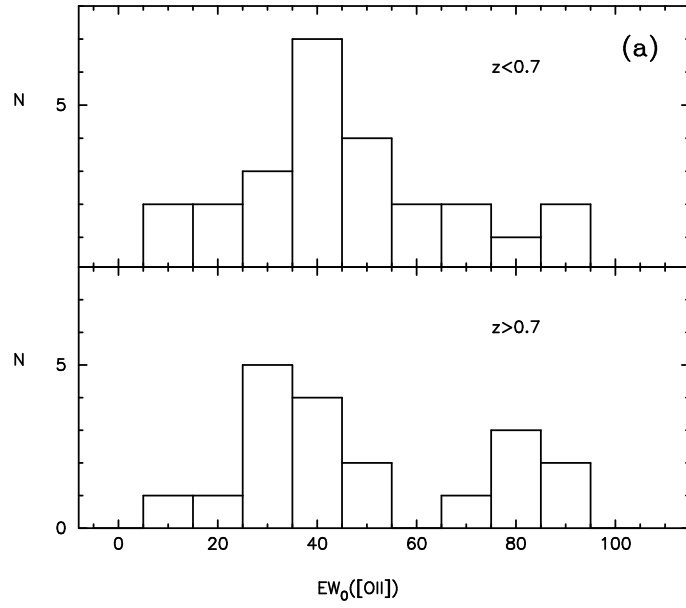




Table 2a. Average spectroscopic parameters for HDF compact galaxies.

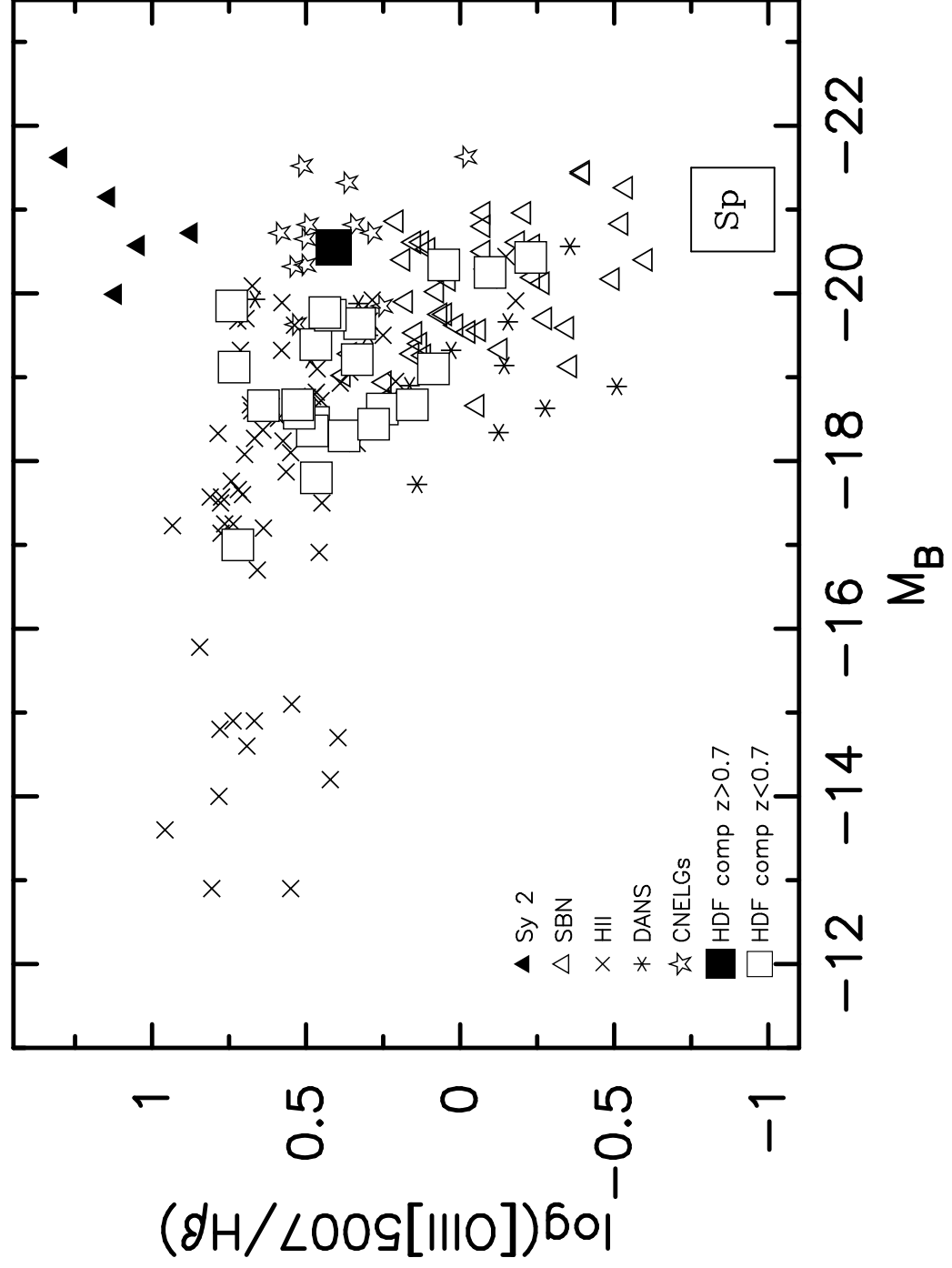
Type (1)	z (2)	W[OII] (3)	$\frac{[OIII]}{H\beta}$ (4)	$\sigma$ (5)	log LH $\beta$ (6)	SFR (7)	N (8)
HII-like	<0.7	55 $\pm$ 5	3.1 $\pm$ 0.3	43 $\pm$ 2	40.5 $\pm$ 0.1	0.8 $\pm$ 0.5	14
HII-like	>0.7	59 $\pm$ 7	2.6 $\pm$ 0.4	68 $\pm$ 6	41.2 $\pm$ 0.1	6.4 $\pm$ 0.5	13
SB disk-like	<0.7	33 $\pm$ 5	2.1 $\pm$ 0.4	69 $\pm$ 5	40.5 $\pm$ 0.1	0.7 $\pm$ 0.9	12
SB disk-like	>0.7	30 $\pm$ 6	...	105 $\pm$ 13	...	2.5 $\pm$ 1.0	6

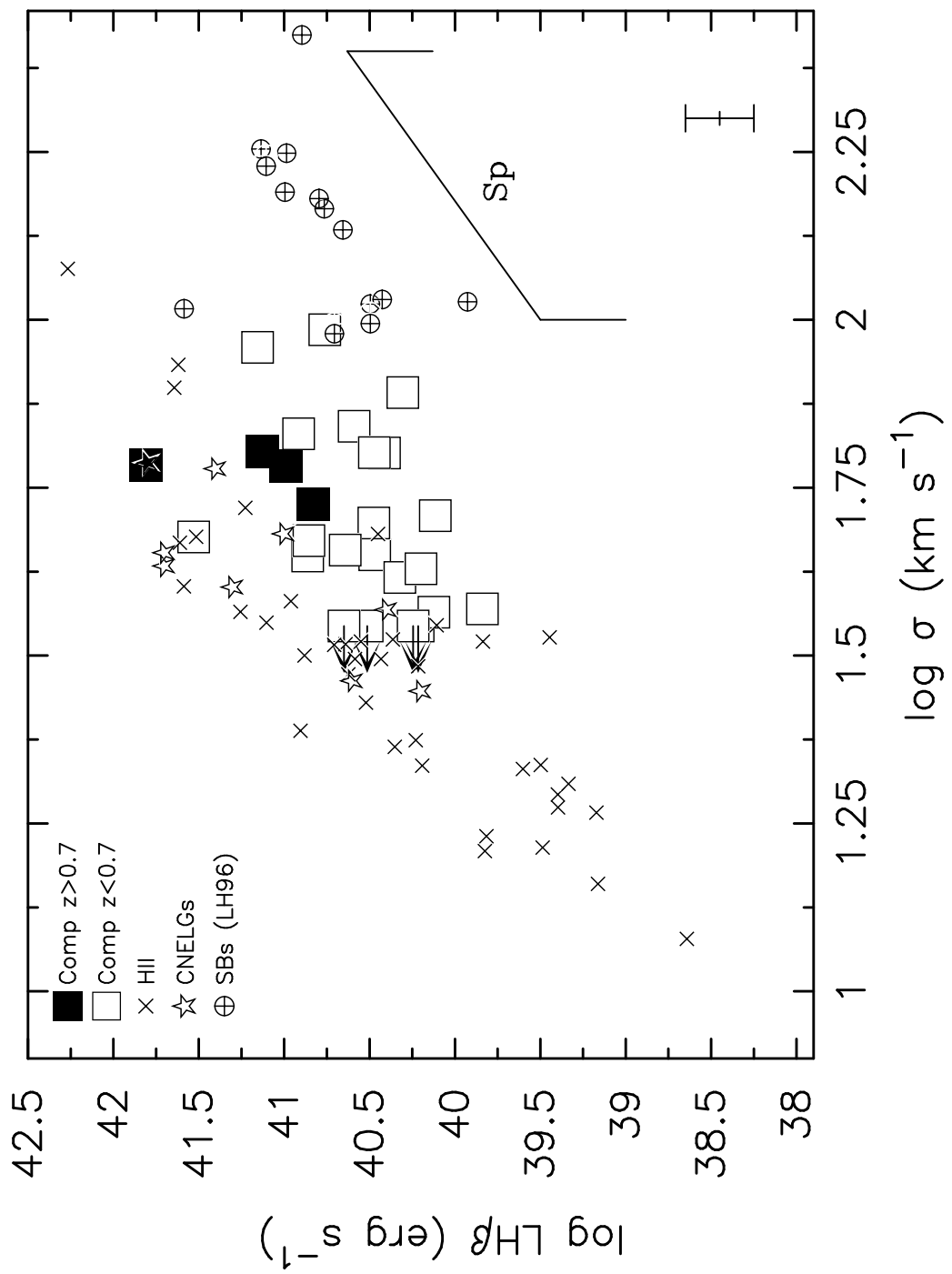
NOTE.— (1) Spectroscopic class; (2) Redshift range; (3) Rest-frame [OII] $\lambda$ 3727 equivalent width in  $\text{\AA}$ ; (4) Observed excitation parameter [OIII]/H $\beta$ ; (5) Line-width (Gaussian sigma) in  $\text{km s}^{-1}$ ; (6) Log of the observed H $\beta$  luminosity in  $\text{erg s}^{-1}$ ; (7) Star formation rate in  $M_{\odot}/\text{yr}$ ; (8) Number of objects within the redshift range. Note that the number of objects used in each column may vary.

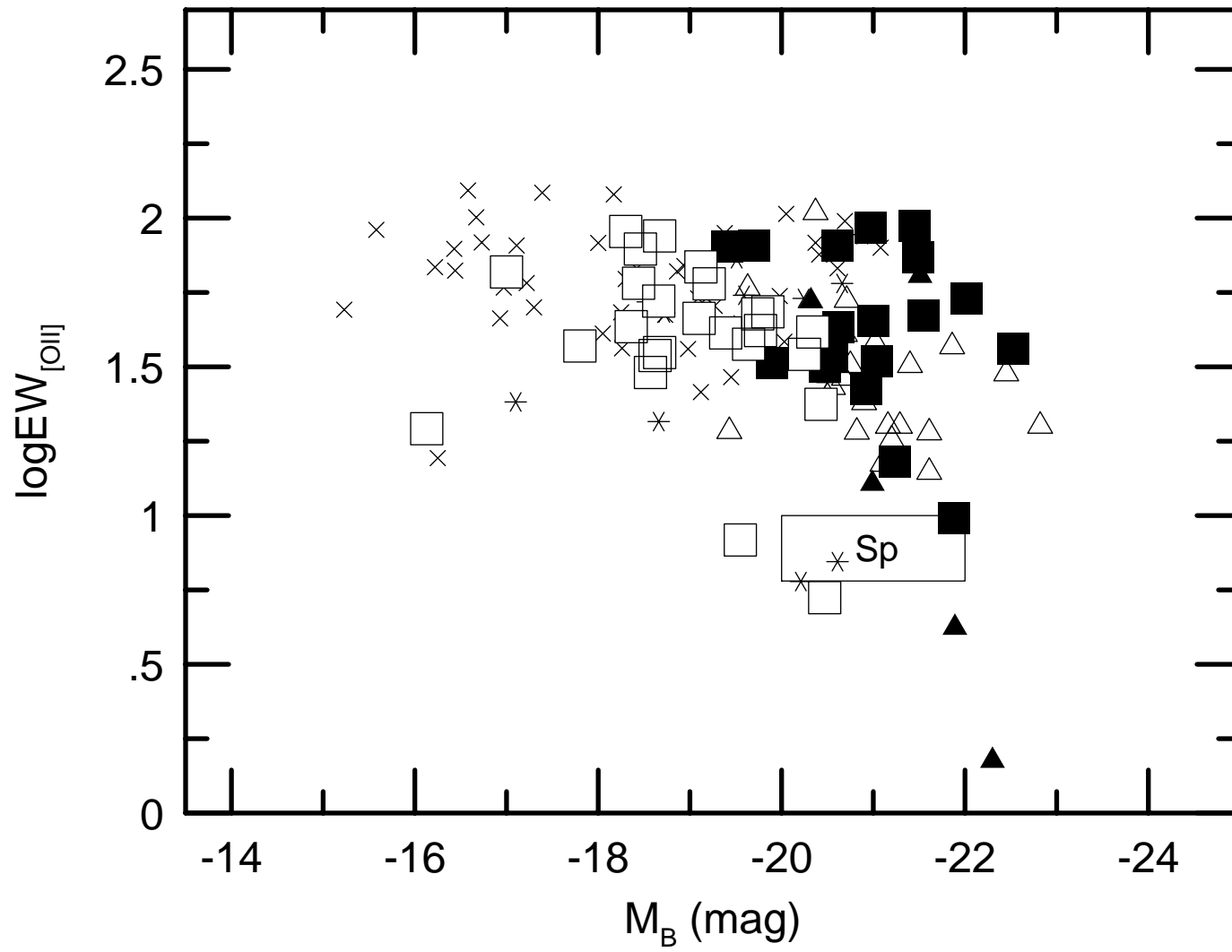
Table 2b. Average structural parameters for HDF compact galaxies.

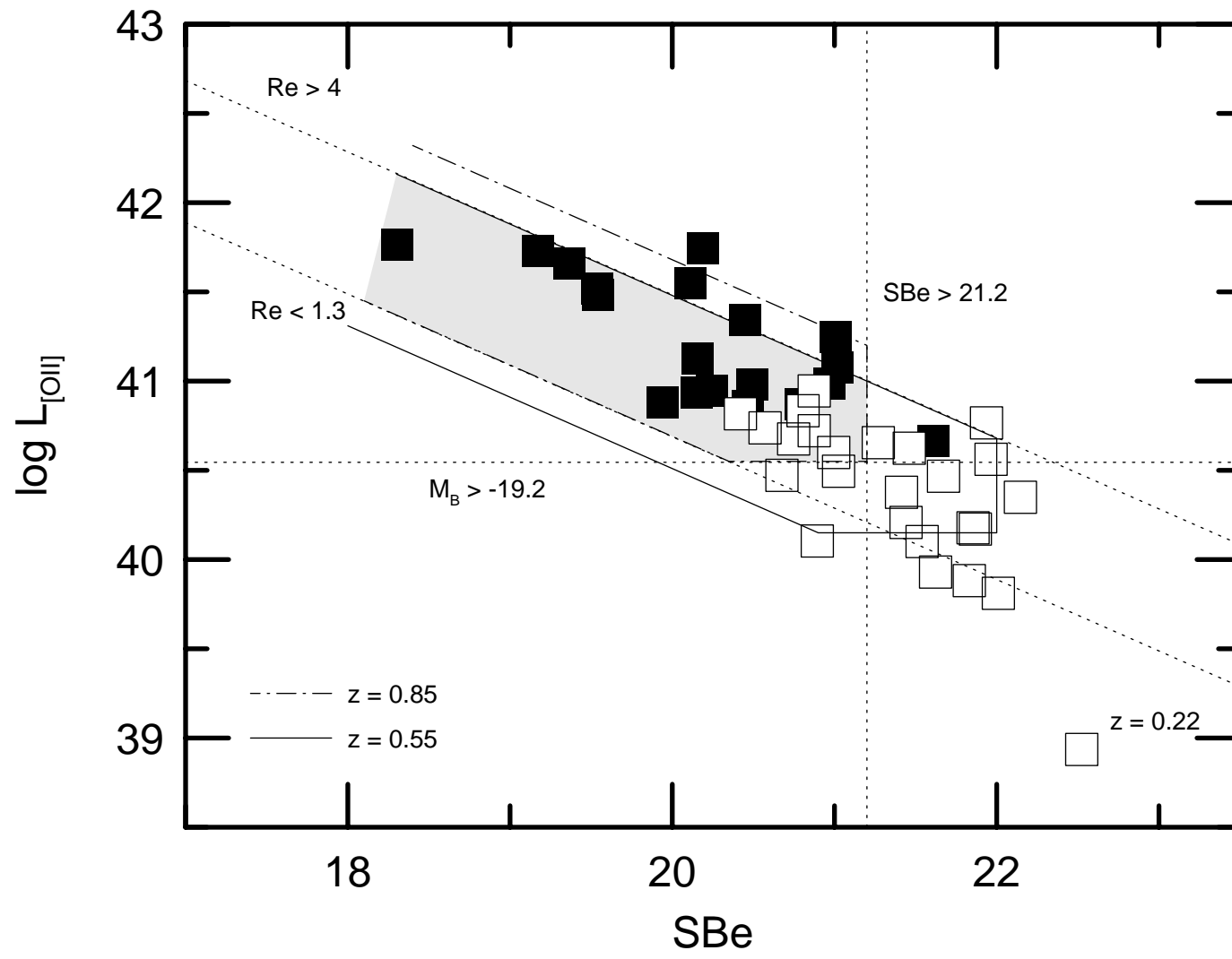
Type (1)	z (2)	$M_B$ (3)	Re (4)	SBe (5)	log M (6)	log SFR/M (7)	M/L (8)	N (9)
HII-like	<0.7	-19.0 $\pm$ 0.2	1.8 $\pm$ 0.2	20.7 $\pm$ 0.2	9.3 $\pm$ 0.1	1.6 $\pm$ 0.1	0.4 $\pm$ 0.1	14
HII-like	>0.7	-21.0 $\pm$ 0.2	2.6 $\pm$ 0.3	19.6 $\pm$ 0.3	9.9 $\pm$ 0.1	1.8 $\pm$ 0.1	0.2 $\pm$ 0.1	13
SB disk-like	<0.7	-19.1 $\pm$ 0.4	2.5 $\pm$ 0.3	21.2 $\pm$ 0.1	9.8 $\pm$ 0.1	0.8 $\pm$ 0.1	1.2 $\pm$ 0.1	12
SB disk-like	>0.7	-21.1 $\pm$ 0.3	4.0 $\pm$ 0.3	20.5 $\pm$ 0.4	10.4 $\pm$ 0.1	1.0 $\pm$ 0.1	0.8 $\pm$ 0.1	6

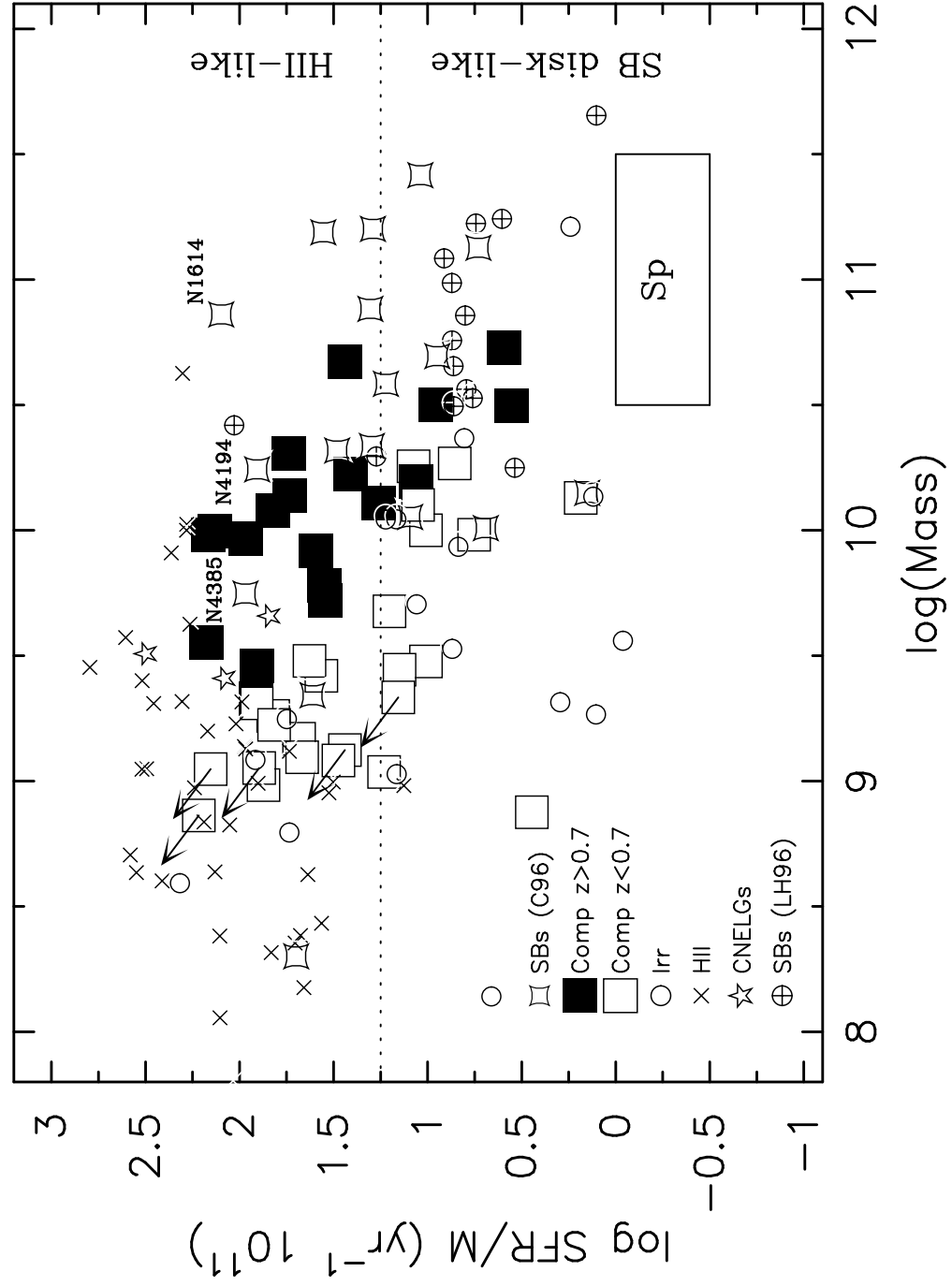
NOTE.— (1) Spectroscopic class; (2) Redshift range; (3) Absolute magnitude in the rest-frame  $B$  band; (4) Half-light radius in Kpc; (5) Rest-frame  $B$  surface brightness in magnitudes per square arcsecond; (6) Log of the mass in solar units; (7) log SFR per unit mass in  $\text{yr}^{-1}$  normalized to  $10^{11}$  solar masses; (8) Mass-to-light ratio in solar units; (9) Number of objects within the redshift range. Note that the number of objects used in each column may vary.

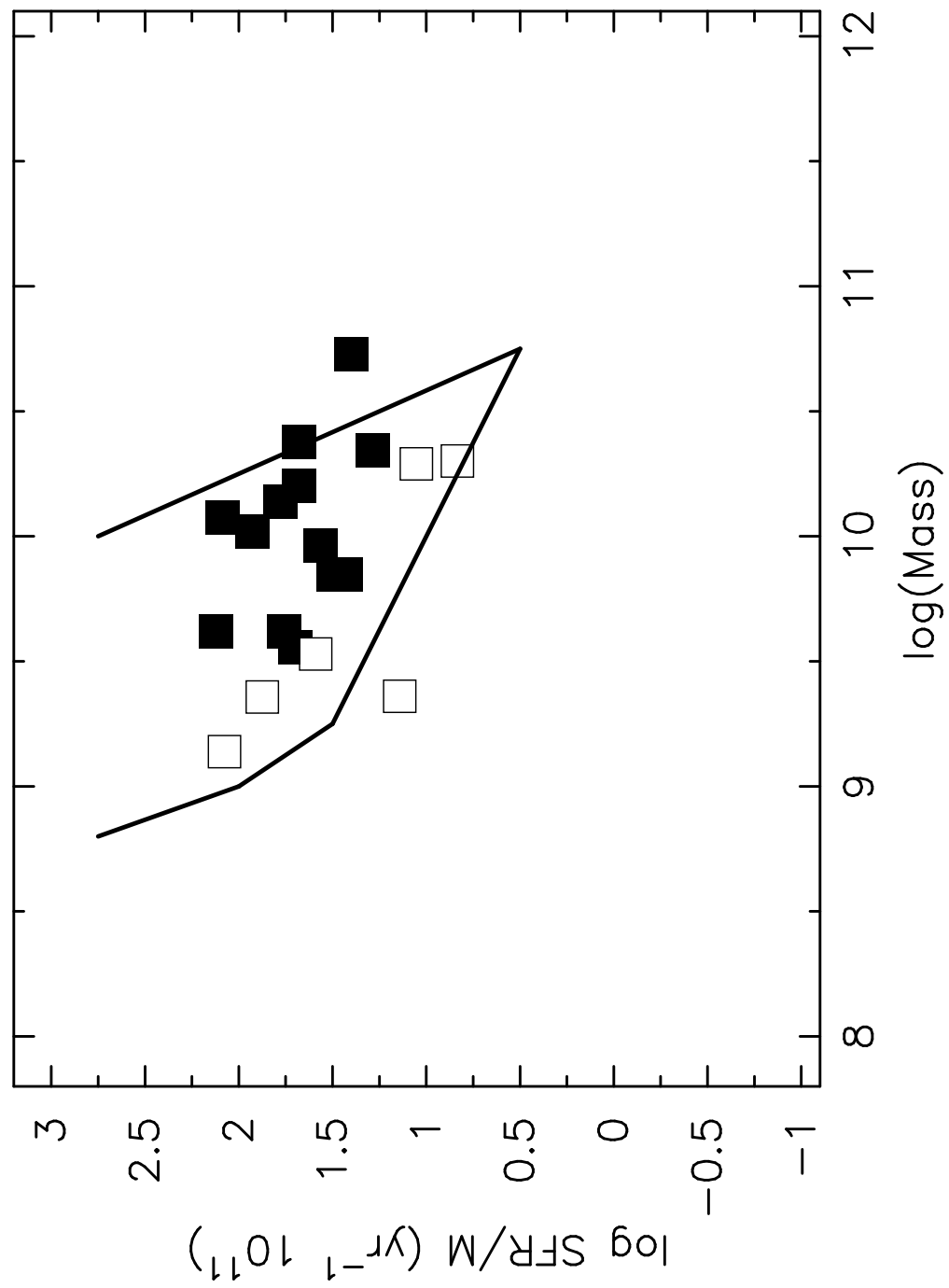


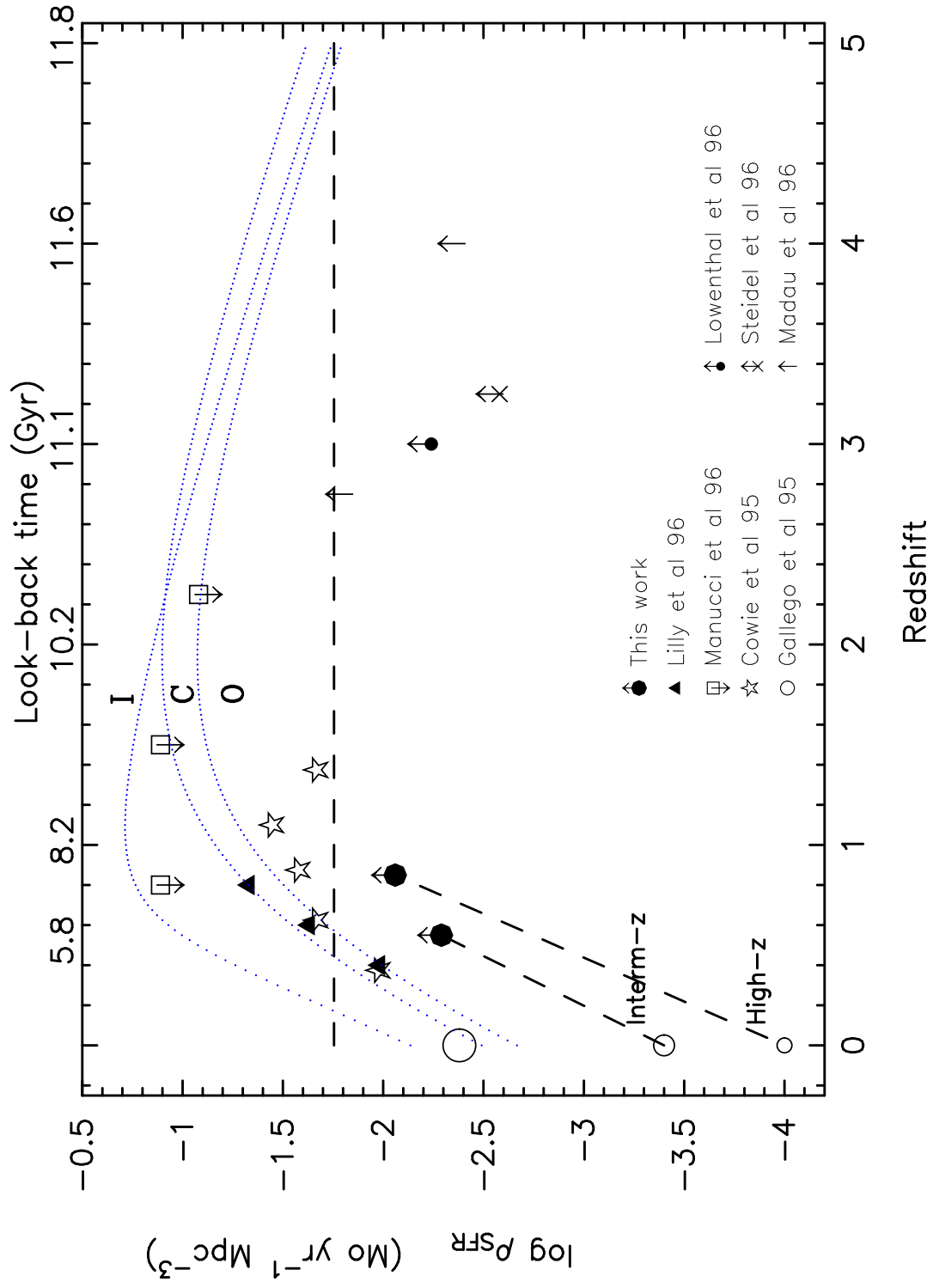














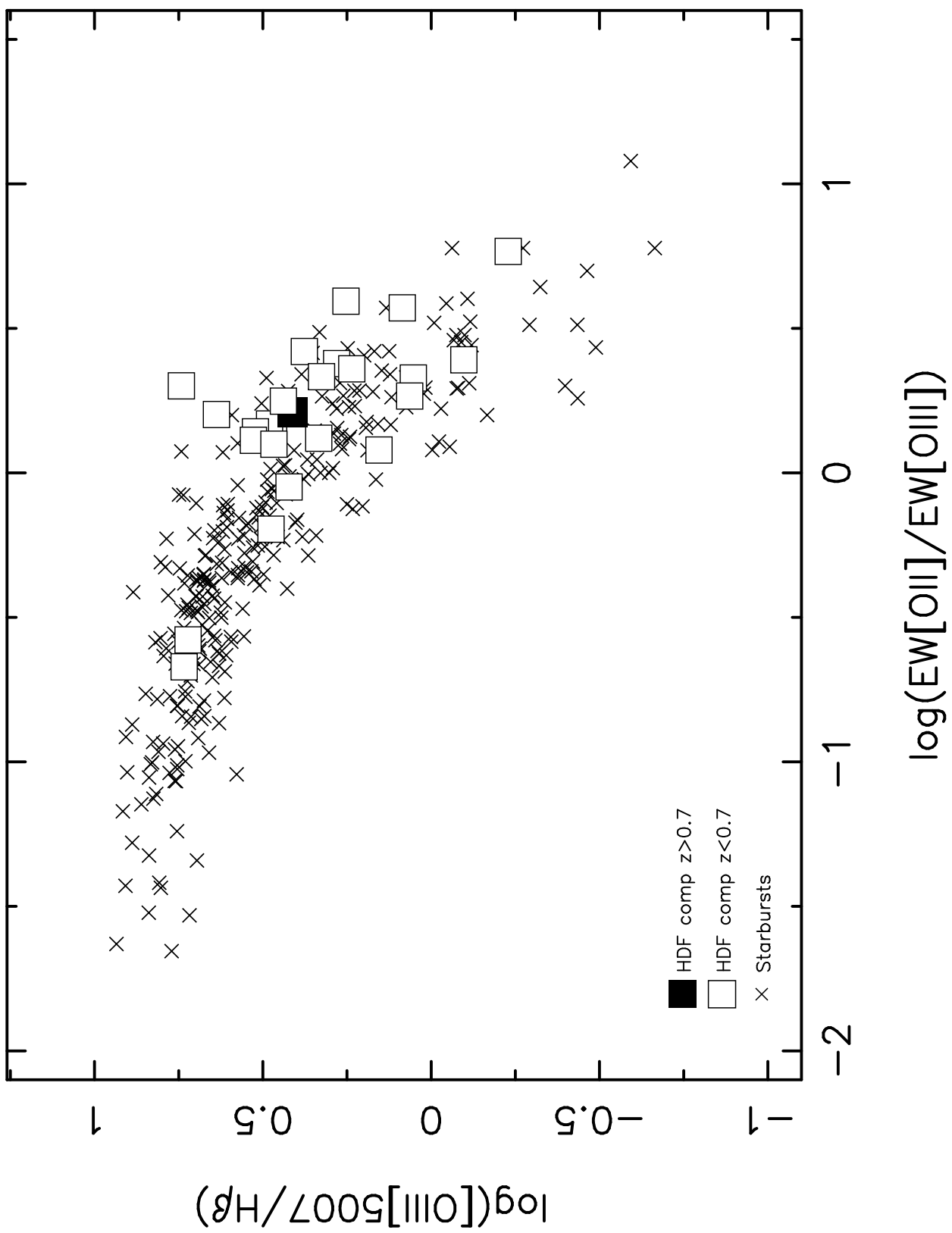


Table 1a. Spectroscopic parameters for HDF compact galaxies.

Object	$I_{814}$	$z$	$W_{[OII]}$	$W_{H\beta}$	$W_{[OIII]}$	$\frac{[OIII]}{H\beta}$	$\sigma$	$L_{H\beta}$	SFR	Type
(1)	(2)	(3)	(4)	(5)	(6)	(7)	(8)	(9)	(10)	(11)
sw3_1455_0476	21.79	0.137	66	48	250	5.27	<35	40.24	1.2	HII-like
se3_0982_0226	23.44	0.224	20	...	11	...	41	...	0.02	SB disk-like
ow3_1047_0444	22.91	0.318	37	9	30	2.93	37	39.84	0.2	HII-like
se3_1090_0023	21.83	0.410	...	...	...	...	...	...	...	E/S0
ne3_1126_0494	22.66	0.420	30	8	22	3.33	51	40.12	0.3	SB disk-like
oe2_0040_0229	22.78	0.423	60	15	25	1.91	78	40.31	0.5	SB disk-like
iw4_1499_0841	23.02	0.437	43	10	29	3.02	37	40.12	0.4	HII-like
nw4_1111_0965	22.44	0.457	46	10	12	1.22	63	40.41	0.8	SB disk-like
iw2_0106_0094	23.09	0.462	79	21	123	2.99	45	40.47	0.7	HII-like
ie3_1071_0351	22.98	0.476	35	10	9	1.79	<35	40.22	0.4	HII-like
oe2_0513_0235	21.09	0.480	24	7	4	0.59	97	40.76	1.3	SB disk-like
sw4_1068_1043	21.90	0.482	42	9	24	2.75	45	40.64	1.3	HII-like
oe4_1100_1320	23.02	0.483	53	9	33	4.35	43	40.20	0.6	HII-like
iw3_1144_0405	23.35	0.485	90	18	34	2.38	41	40.32	0.7	HII-like
oe3_0801_0291	21.97	0.487	38	9	17	2.12	69	40.59	1.0	SB disk-like
nw2_0557_0629	22.15	0.503	...	...	...	...	...	...	...	E/S0
iw2_0186_0458	22.41	0.507	41	10	30	2.94	<35	40.51	0.9	HII-like
sw3_1378_0453	21.12	0.509	5	5	...	...	<35	40.67	0.3	SB disk-like
se4_0940_1478	22.62	0.513	60	26	46	2.16	47	40.85	1.1	HII-like
iw4_1173_1391	20.84	0.519	...	...	...	...	...	...	...	E/S0
ow3_1063_0391	23.23	0.528	35	18	29	1.43	50	40.47	0.4	SB disk-like
nw4_1278_1205	20.57	0.558	...	...	...	...	...	...	...	E/S0
ie4_1442_1007	21.13	0.560	11	7	...	...	117	40.89	0.8	SB disk-like
ne3_0969_0527	22.19	0.570	8	...	...	...	79	...	0.2	SB disk-like
nw4_0920_1247	22.21	0.570	48	9	24	5.52	<35	40.65	1.6	HII-like
ie3_0998_0401	21.81	0.594	41	18	19	1.13	91	41.16	2.1	SB disk-like
se2_0673_0133	22.44	0.594	48	18	53	2.64	68	40.92	1.4	SB disk-like
ow3_1308_0563	23.73	0.654	87	18	67	3.37	63	40.47	1.0	HII-like
ne3_1323_0484	21.69	0.677	...	...	...	...	...	...	...	E/S0
ow3_1376_0297	22.28	0.693	35	10	14	0.80:	44	40.86	1.7	HII-like
ie3_1030_0507	23.44	0.693	69	132	321	5.42	47	41.53	1.2	HII-like

NOTE.— (1) Object ID: (field,CCD)-(x)-(y), with x and y in pixels; (2) Total  $I_{814}$  magnitude zero-pointed to Vega; errors are estimated to be  $\pm 0.05$ mag (see Paper I); (3) Redshift, with uncertainty  $\lesssim 0.001$ ; (4) Rest-frame  $[OII]\lambda 3727$  equivalent width in  $\text{\AA}$  (errors  $\sim 15\%$ ); (5) Rest-frame  $H\beta$  equivalent width in  $\text{\AA}$  (errors  $\sim 15\%$ ); (6) Rest-frame  $[OIII]\lambda 5007$  equivalent width in  $\text{\AA}$  (errors  $\sim 15\%$ ); (7) Observed excitation parameter  $[OIII]/H\beta$  (errors  $\sim 25\%$ ); (8) Line-width (gaussian sigma), in restframe km/s (typical uncertainty  $\sim 20\%$ ); (9) Log of the observed  $H\beta$  luminosity in  $\text{erg/s}$  ( $\pm 0.1$  uncertainty); (10) Total SFR in  $M_{\odot} \text{ yr}^{-1}$  (errors  $\sim 15\%$ ); (11) Spectroscopic type, with HII-like being those with  $\log(SFR/M) > 1.25$  and SB disk-like those with  $\log(SFR/M) < 1.25$ . The values marked with ':' are very uncertain ( $\sim 50\%$ ).

Table 1b. Spectroscopic parameters for HDF compact galaxies. Continued.

Object	I <sub>814</sub>	z	W <sub>[OII]</sub>	W <sub>H<math>\beta</math></sub>	W <sub>[OIII]</sub>	$\frac{[OIII]}{H\beta}$	$\sigma$	L <sub>H<math>\beta</math></sub>	SFR	Type
(1)	(2)	(3)	(4)	(5)	(6)	(7)	(8)	(9)	(10)	(11)
nw3_1434_0108	22.82	0.744	33	...	...	...	112	...	1.1	SB disk-like
sw4_0807_1067	22.24	0.760	34	10	21	2.58	61	40.99	2.1	HII-like
oe3_1089_0455	21.84	0.784	33	9	...	...	64	41.13	3.3	HII-like
ie3_1025_0359	23.49	0.788	80	20	...	...	53	40.83	1.8	HII-like
oe4_1223_1134	22.05	0.821	93	...	...	...	68	...	8.6	HII-like
ne3_0769_0583	21.60	0.840	74	...	...	...	109	...	11.0	HII-like
se2_0021_0728a	22.20	0.845	27	...	...	...	65	...	2.3	SB disk-like
nw4_0770_1239	22.13	0.847	45	...	...	...	72	...	4.3	HII-like
nw2_0367_0766	21.00	0.873	...	...	...	...	...	...	...	E/S0
iw4_1212_1333	23.55	0.880	81	...	...	...	53	...	2.3	HII-like
ne4_1136_1005	22.94	0.898	32	...	...	...	65	...	1.8	HII-like
se4_1387_0990	22.78	0.905	43	...	...	...	109	...	2.9	SB disk-like
ie3_1443_0559	21.91	0.907	94	29	...	...	61	41.81	13.5	HII-like
oe2_0168_0249	22.23	0.909	15	...	...	...	69	...	1.8	SB disk-like
oe4_1109_1148	21.47	0.936	54	...	...	...	151	...	13.0	SB disk-like
se2_0309_0594	21.79	0.936	10	...	...	...	128	...	2.1	SB disk-like
ne4_1292_0943	23.29	1.050	80	...	...	...	43	...	5.3	HII-like
oe2_0342_0725	22.74	1.084	47	...	...	...	84	...	7.4	HII-like
iw4_1002_1353	22.17	1.221	36	...	...	...	77	...	14.1	HII-like
iw2_0497_0674	23.00	1.344	43	...	...	...	75	...	8.0	HII-like

NOTE.— (1) Object ID: (field,CCD)-(x)-(y), with x and y in pixels; (2) Total I<sub>814</sub> magnitude zero-pointed to Vega; errors are estimated to be  $\pm 0.05$  mag (see Paper I); (3) Redshift, with uncertainty  $\lesssim 0.001$ ; (4) Rest-frame [OII] $\lambda 3727$  equivalent width in  $\text{\AA}$  (errors  $\sim 15\%$ ); (5) Rest-frame H $\beta$  equivalent width in  $\text{\AA}$  (errors  $\sim 15\%$ ); (6) Rest-frame [OIII] $\lambda 5007$  equivalent width in  $\text{\AA}$  (errors  $\sim 15\%$ ); (7) Observed excitation parameter [OIII]/H $\beta$  (errors  $\sim 25\%$ ); (8) Line-width (Gaussian sigma) in  $\text{km s}^{-1}$  (typical uncertainty  $\sim 20\%$ ); (9) Log of the observed H $\beta$  luminosity in  $\text{erg s}^{-1}$  ( $\pm 0.1$  dex uncertainty); (10) Total SFR in  $M_{\odot} \text{ yr}^{-1}$  (errors  $\sim 15\%$ ); (11) Spectroscopic type.